https://doi.org/10.5194/egusphere-2026-6959
Preprint. Discussion started: 20 November 2026
© Author(s) 2026. CC BY 4.0 License.

Fireworks promote the secondary formation of atmospheric imidazoles rather than their direct emission: Insights from firework source samples and machine learning

Chen Chen[1], Weibo Li[1], Jierui Hou[1], Qizong Wang[1,] Xiaodi Liu[1,2,3], Can Wu[3], Xin Zhang[1,2], Zhanfang Hou[1,2], Jingjing Meng[1,2]

[1] School of Geography and Environment, Liaocheng University, Liaocheng 252000, China
[2] Institute of Huanghe Studies, Liaocheng University, Liaocheng 252000, China
[3] School of Geographic Sciences, Key Lab of Geographic Information Science of the Ministry of Education, East China Normal University, Shanghai 200241, China

Correspondence to: Jingjing Meng (mengjingjing@lcu.edu.cn)

Abstract: Firework emissions release large quantities of reactive nitrogen- and carbon-containing species that can modify aerosol chemical evolution, yet their impacts on imidazole-containing particles remain poorly constrained. In this work, single-particle aerosol mass spectrometry was deployed to probe imidazole evolution during the firework (FW) episode in Liaocheng, China, combined with source sample experiments and multi-model machine learning analysis. Field observations revealed pronounced elevations in particle counts and fractional contributions of imidazoles during the FW episode, along with a shift from bimodal to trimodal particle-size distribution and strengthened internal mixing with sulfate, nitrate, and ammonium. Analysis of firework source samples confirmed no direct imidazole emissions from fireworks, yet abundant precursors of imidazoles (including amines, ammonium, and carbonyl compounds) were detected. Machine learning attribution identified carbonyl compounds and amines as predominant drivers for imidazole formation, with modified particle acidity acting as a secondary modulator, whereas inorganic salts, relative humidity, and NO_x exerted largely indirect regulatory effects. Photochemical degradation driven by O_3 constituted a major atmospheric sink for imidazoles. This study demonstrates that fireworks predominantly boost the secondary production of imidazoles rather than direct primary emissions, which advances mechanistic insights into episodic brown-carbon evolution and nitrogen-heterocycle aerosol pollution driven by intense short-term combustion events.

https://doi.org/10.5194/egusphere-2026-6959
Preprint. Discussion started: 20 November 2026
© Author(s) 2026. CC BY 4.0 License.

1 Introduction

As widespread nitrogen heterocycles found in atmospheric particulate matter, imidazole particles make up a major portion of brown carbon (BrC) and possess pronounced light-absorbing properties, thereby disturbing atmospheric radiative balance (Laskin et al., 2025; Xiao et al., 2025; Zhu et al., 2022). Certain imidazole species, including 2,2′-biimidazole and imidazole-2-carboxaldehyde, can function as photosensitizers and may initiate diverse reactions within aerosol particles (Hu et al., 2022; Tinel et al., 2014). Besides, a subset of these compounds (such as 2-methylimidazole and 4-methylimidazole) pose potential carcinogenic risks to humans and are designated as Group 2B carcinogens (Hu et al., 2022). Imidazole particles stem from both primary emissions (e.g., biomass burning) and secondary transformation pathways (e.g., heterogeneous or aqueous reactions) (Gao et al., 2021). The well-documented formation route proceeds via the reactions of glyoxal (Gly) or methylglyoxal (mGly) with amines, amino acids, or ammonium in aerosol liquid water, producing imidazole products (De Haan et al., 2019; Shen et al., 2023). Field measurements have revealed distinct diurnal variations in imidazole-containing particles, with generally higher nighttime counts relative to daytime levels, which are tightly linked to their photochemical degradation initiated by O_3 and ·OH radicals (Hu et al., 2022; Teich et al., 2016). Laboratory experiments and theoretical calculations further demonstrate that atmospheric imidazoles have relatively short lifetimes, as they are prone to photodegradation via reaction with O_3 and ·OH radicals, with photolysis acting as another critical sink (Wei et al., 2024).

The formation and loss processes of imidazoles can be substantially altered under episodic pollution conditions with abundant reactive precursors. As a prominent type of episodic combustion source, firework displays create a distinct chemical environment that differs from ambient background conditions (Ke et al., 2026; Klapötke et al., 2010; Liu et al., 2026) and may reshape the production and evolution of imidazoles. Fireworks can emit abundant gaseous and particulate pollutants, including hydrocarbon compounds, inorganic salts (e.g., potassium, perchlorate, nitrate, and sulfate), carbonaceous species, and metals (e.g., barium (Ba), magnesium (Mg), strontium (Sr), copper (Cu) and chlorine (Cl)) (Do et al., 2012; Huang et al., 2024). These components can change physicochemical conditions of aerosols, such as increasing aerosol liquid water content (ALWC) and adjusting particle acidity within firework plumes, which are theoretically favorable for the aqueous reactions producing imidazoles (Wu et al., 2018a). Many field campaigns have recorded elevated BrC and nitrogen-containing organic signals during firework events (Gui et al., 2025; Tripathi et al., 2026). Our previous field and source-simulation observations further demonstrate that firework emissions substantially enhance amine-containing particles, in which modified aerosol acidity and ALWC acted as key regulators governing gas-particle partitioning and heterogeneous reactions of amine-containing particles in the firework (FW) episode (Chen et al., 2026a). Nevertheless, few attempts have been made to investigate the direct primary emissions of imidazoles from firework discharges and their secondary formation mechanisms, as well as the key influencing factors. This knowledge gap constrains reliable evaluation of BrC radiative impacts during the FW episode.

Traditional filter-based offline measurements yield averaged signals by mixing particles with distinct origins and chemical histories through bulk aerosol analysis (Robinson et al., 2013), thus it cannot identify whether imidazole signals belong to

https://doi.org/10.5194/egusphere-2026-6959
Preprint. Discussion started: 20 November 2026
© Author(s) 2026. CC BY 4.0 License.

freshly emitted firework particles or particles formed through subsequent aqueous reactions. Single-particle mass spectrometry can resolve chemical information of individual particles and enables the separation of particle populations with different formation pathways (Lian et al., 2021). Additionally, analysis of firework source samples can provide characteristic reference spectral fingerprints of freshly emitted primary particles and enable direct comparison with ambient particles sampled within firework plumes (Chen et al., 2026a). However, spectral interference from complex mixtures in firework plumes hinders reliable manual classification of particle types. Machine learning algorithms serve as powerful tools to decode hidden spectral information from large single-particle datasets and help identify key factors governing imidazole formation in the FW episode (Chen et al., 2026a; Hu et al., 2022; Xu et al., 2025). This combined analytical strategy integrating source sample characterization, single-particle mass spectrometry, and machine learning advances our understanding of imidazoles influenced by intense firework pollution.

This study integrates field observations covering FW and non-FW (NFW) periods to resolve the sources, mixing states, and evolutionary mechanisms of imidazole-containing particles using single-particle mass spectrometry alongside firework source samples and machine learning approaches. We test the core hypothesis that firework emissions promote the secondary formation of atmospheric imidazoles instead of serving as a direct emission source of these species. We further compare the chemical features of imidazole-containing particles across FW and NFW periods to identify key controlling factors driving imidazole production within firework plumes. The findings improve our understanding of episodic BrC evolution and nitrogen heterocycle formation under intense short-term combustion perturbations.

2 Materials and methods

2.1 Field Measurements

Field measurements were conducted at Liaocheng University (36.43°N, 116.01°E) in southeastern Liaocheng, Shandong Province, China. As a key city for air pollution prevention and control under the "2 + 36" framework, Liaocheng experiences frequent and severe air pollution, especially during winter. The monitoring site is surrounded by densely populated residential zones and busy roads but is free of tall structures or industrial plants, making it ideal for assessing urban air quality (Ma et al., 2024). The sizes and chemical signatures of individual particles were analyzed hourly using a single-particle aerosol mass spectrometer (Model 0515-R, Hexin Instrument Co., Ltd., Guangzhou, China), operated at an airflow rate of 75 mL·min^{-1} via an inlet mounted on the top of a six-floor structure. Meteorological parameters and key atmospheric pollutants (e.g., PM_{10}, $PM_{2.5}$, SO_2, CO, O_3, and NO_x) were monitored concurrently throughout the SPAMS measurement campaign. Based on monitoring data and local cultural traditions, the intensive FW episode was designated as 18:00 on 21 January to 17:00 on 23 January 2023. The NFW episode is defined as all other sampling intervals during the whole observation episode.

https://doi.org/10.5194/egusphere-2026-6959
Preprint. Discussion started: 20 November 2026
© Author(s) 2026. CC BY 4.0 License.

2.2 Data analysis

2.2.1 SPAMS data

A detailed description of the SPAMS has been available in Chen et al. (2023) and Ma et al. (2024). Briefly, particles were sampled via a $PM_{2.5}$ inlet and dried using a silica gel dryer prior to introduction into the SPAMS. Particles were subsequently focused through an aerodynamic lens and traversed two continuous Nd:YAG laser beams (532 nm) for velocity determination. Based on the measured velocities, a timed ultraviolet laser pulse (266 nm) was triggered downstream to achieve desorption and ionization of individual particles. The resulting positive and negative ion fragments were then detected. The vacuum aerodynamic diameter of each particle was derived from its measured velocity, calibrated against monodisperse polystyrene latex microspheres (Duke Scientific Corp., Palo Alto, CA) spanning a size range of 0.22–2.0 μm. The SPAMS dataset was subjected to analysis with the COCO toolkit version 3.0, operating within MATLAB 2014b (MathWorks Inc., USA). The hourly averaged number fraction (Nf) and relative peak area (RPA) were employed as metrics to track temporal variations of particle constituents. Here, RPA is defined as the percentage of a target ion's peak area relative to the sum of all peak areas. Following established methods (Hu et al., 2022), imidazole-containing particles were identified by detecting characteristic ions at *m/z* $^{69}(C_3H_4N_2H)^+$, $^{81}(C_4H_5N_2)^+$, $^{97}(C_5H_8N_2H)^+$/$^{97}(C_4H_4N_2OH)^+$, and $^{134}(C_6H_6N_4)^+$, when the peak area of any of these ions exceeded 50 (Table 1). Potential interferences from Zn-containing particles (*m/z* 64, 66, or 68) and sea salt (*m/z* 23, 62, or 81) were excluded during the analysis. As crucial precursors of imidazole-containing particles, carbonyl compounds were characterized by the presence of signature fragments at *m/z* $^{71}[C_3H_3O_2]^-$ (mGly) and $^{73}[C_2HO_3]^-$ (Gly) (Hamilton et al., 2013; Zauscher et al., 2013). Likewise, ammonium was detected by *m/z* $^{18}[NH_4]^+$, while amine-containing particles served as markers at *m/z* $^{30}[CH_3NH]^+$ (MA), $^{74}[(C_2H_5)_2NH_2]^+$ (DEA), or $^{86}[(C_2H_5)_2NCH_2]^+$/ $^{101}[(C_2H_5)_3N]^+$ (TEA) (Li et al., 2021; Cheng et al., 2018; Angelino et al., 2001).

2.2.2 Calculation of ALWC, relative aerosol acidity (R_{ra}), and modified R_{ra} (R_{ra}')

In this study, real-time concentrations of water-soluble inorganic ions were acquired at hourly resolution using an MARGA Ion Analyzer ADI 2080 (Applikon Analytical B.V., the Netherlands). Combined with these ion measurements and key meteorological variables, including relative humidity (RH) and temperature, ALWC was calculated using the ISORROPIA-II model (Shen et al., 2025). R_{ra} is defined as the ratio of the total peak areas of nitrate and sulfate to the ammonium peak area and has been validated as reliable in multiple previous studies (Denkenberger et al., 2007; Huang et al., 2013; Meng et al., 2021). Considering the basicity of amines, this work refined R_{ra} following the approach reported by Cheng et al. (2017), to derive R_{ra}'.

https://doi.org/10.5194/egusphere-2026-6959
Preprint. Discussion started: 20 November 2026
© Author(s) 2026. CC BY 4.0 License.

2.3 Treatment of firework source samples

To determine whether imidazoles can be directly emitted from fireworks, firework source samples were collected. $PM_{2.5}$ samples were obtained in the combustion laboratory with a dilution sampling system (TH-150, Tianhong Ltd., China) running at 16.7 L min^{-1}. Forty $PM_{2.5}$ source samples were collected from twenty types of firecrackers and twenty categories of fireworks, which are grouped together as firework source samples.

Quantification of imidazoles in $PM_{2.5}$ followed an established analytical protocol reported in prior work (Liu et al., 2023). In brief, a quarter of each filter was extracted using 5 mL ultrapure water containing 1% *v*/*v* methanol under sonication for 1 h. The extract was passed through a 0.22 μm PTFE syringe filter to eliminate insoluble particulates, then analyzed using a high-performance liquid chromatography (HPLC, Thermo Scientific) interfaced to an Orbitrap mass spectrometer (MS, Thermo Scientific). Chromatographic separation was performed on an ACQUITY UPLC HSS T3 column (100 mm × 2.1 mm, 1.8 μm; Waters Corporation, Milford). Since these imidazole compounds constitute the most abundant imidazole fraction observed in ambient air (Hu et al., 2022), five standard solutions (Sigma-Aldrich) of imidazole-2-carboxaldehyde (IC), 2,2′-biimidazole (BM), 2-ethylimidazole (EI), 2,4-dimethylimidazole (DMI), and 4-methylimidazole (MIM) were prepared and measured via HPLC-MS to acquire retention time and mass information for subsequent sample identification. In addition, an aliquot from each source sample underwent three sequential ultrasonic extractions with 10 mL Milli-Q water for 15 min per extraction. The resulting extracts were introduced into a TSI 9302 aerosol generator to generate aerosols at 10 psi and a flow rate of 3.7 L min^{-1}. These aerosols passed through a silica gel drying tube before SPAMS characterization to identify imidazoles in source samples. The above five standard reagents were nebulized and introduced into the SPAMS to identify ion markers for imidazole-containing particles.

2.4 Machine learning model construction

To quantitatively simulate concentrations of imidazoles and identify key driving factors, we constructed six base models spanning linear and nonlinear categories, and further developed a dynamically weighted ensemble model for performance comparison. Linear models consisted of Ridge regression, Huber robust regression, and partial least squares regression (PLSR). Nonlinear models included Gaussian process regression (GPR), support vector regression (SVR), and gradient boosting regression (GBR). In addition, to evaluate the gain from ensemble strategies, two schemes were developed, with a dynamically weighted ensemble based on inverse mean squared error (Ensemble_New) as the improved strategy and a simple average ensemble (Ensemble_Old) as the benchmark (Ravikumar et al., 2025; Stock and Watson, 2004). Given the pronounced right-skewed distribution and heteroscedasticity for counts of imidazole-containing particles at high levels, a logarithmic transformation was applied to the target variable to stabilize variance and mitigate the influence of extreme values. All input predictors were standardized using Z-scores to eliminate dimensional differences that could affect kernel methods and regularization models. The dataset was split chronologically into training and test sets to avoid information leakage.

https://doi.org/10.5194/egusphere-2026-6959
Preprint. Discussion started: 20 November 2026
© Author(s) 2026. CC BY 4.0 License.

For ridge regression, L_2 regularization was employed to constrain regression coefficients, thereby mitigating the risk of overfitting and stabilizing parameter estimates under multicollinearity and providing a robust linear baseline for environmental datasets with limited sample sizes (Bendersky and Fridkin, 2026). Huber regression replaced the least-squares loss with the Huber loss, reducing sensitivity to high-concentration outliers and alleviating the influence of extreme pollution events on parameter estimation (Lawrence and Bhathmanabhan, 2026). PLSR performed simultaneous dimensionality reduction and regression via latent variable decomposition, maintaining stable prediction under highly correlated features and providing variable importance in projection (VIP) scores for feature interpretation (Wold et al., 2001). Among the nonlinear models, GPR, based on a Bayesian nonparametric framework, provided not only point predictions but also 95% prediction intervals, enabling uncertainty quantification across different concentration levels (Gündoğdu and Elbir, 2026; Naslidnyk et al., 2025). SVR mapped samples into a high-dimensional feature space using a radial basis function kernel, capturing potential nonlinear responses under strong regularization (Smola and Schölkopf, 2004). GBR sequentially integrated shallow decision trees to approximate the target function, showing the ability to characterize nonlinearity and interactions among variables (Friedman, 2001). To assess the contribution of each variable to the model output, permutation importance was further employed. For the ensemble models, Ensemble_New adopted an inverse mean squared error dynamic weighting strategy. During rolling prediction, weights were dynamically assigned based on the logarithmic-scale prediction errors of each base model within a recent sliding window, so that models with smaller errors received higher ensemble weights. This adaptively suppressed the influence of failing base models under gradually shifting covariates in time series scenarios. Ensemble_Old took a simple arithmetic average of all base models as a control for evaluating ensemble strategy effectiveness.

Model performance was evaluated using the coefficient of determination (R^2), root mean square error (RMSE), and mean absolute error (MAE), assessed on both the original scale and the logarithmic scale. The original-scale metrics reflect the model's simulation accuracy for actual concentrations, while the logarithmic-scale metrics more fairly reflect the model's relative predictive ability in the low-concentration range, preventing high-value samples from dominating the overall error evaluation. All models were implemented using the Python scikit-learn library. Detailed hyperparameter settings, convergence checks, usability assessments, and test set performance summaries are provided in Text S1.

3 Results and discussion

3.1 Air quality deterioration and aerosol physicochemical evolution induced by firework displays

Our previous study confirmed the critical contribution of firework discharges to air quality degradation, as evidenced by elevated $PM_{2.5}$ and PM_{10} concentrations together with higher hourly counts of total single particles in the FW episode relative to the NFW episode, reflecting intense pollution dominated by particles triggered by firework activities (Chen et al., 2026a). As shown in Table 2 and Fig. 1, SO_2 and CO concentrations displayed obvious temporal increases in the FW episode, further

https://doi.org/10.5194/egusphere-2026-6959
Preprint. Discussion started: 20 November 2026
© Author(s) 2026. CC BY 4.0 License.

supporting that firework emissions serve as the dominant driver for the observed air quality deterioration, given that carbon and sulfur are essential constituents of pyrotechnic materials (Liu et al., 2026; Steinhauser and Klapötke, 2008). Cl enrichment arises from thermal decomposition of conventional oxidants within pyrotechnic mixtures such as $KClO_3$ and $KClO_4$, which liberate oxygen and yield KCl during decomposition (Tang et al., 2016). Cu serves as a pyrotechnic pigment that produces blue and green flame emissions for fireworks (Lin, 2016). Accordingly, the particle counts of Cl and Cu in the FW episode increased by 280% and 47.5%, respectively, relative to the NFW episode (Table 2). Sr and Ba are key colorants in pyrotechnic mixtures for producing red and green flames, respectively (Juknelevicius et al., 2015; Ouyang et al., 2022; Sabatini et al., 2015). Consistent with their wide application in firework formulations, particle counts of Sr and Ba all showed substantial elevations in the FW episode compared to the NFW episode (Table 2). From an hourly temporal perspective, all these chemical species exhibited sharp surges starting at 0:00 on 22 January (Chinese New Year's Eve) and reached their peak values between 2:00 and 4:00 (Fig. S1), a timeframe corresponding precisely to the peak concentrated firework burning period. The above findings confirm the dominant role of firework displays in elevating aerosol pollutants in ambient air.

Laboratory studies and field measurements have demonstrated that imidazoles can be formed through the aqueous reactions of carbonyl compounds (e.g., Gly and mGly) with ammonium or amines (Lian et al., 2021; Lin et al., 2015; Powelson et al., 2014). As key precursors of imidazoles, the particle counts of Gly, mGly, ammonium, and amines in the FW episode increased by factors of 0.7, 1.6, 1.6, and 0.9 relative to the NFW episode (Table 2), implying that elevated imidazole–containing particles in the FW episode were likely driven by the enhanced availability of these precursors. Nitrate and sulfate also exhibited substantially higher particle counts in the FW episode, being 1.7- and 1.5-fold higher relative to the NFW episode, respectively (Table 2). Defined as the ratio of combined peak areas of nitrate and sulfate to that of ammonium, R_{ra} has been employed to assess the acidic environment of single particles (Huang et al., 2013; Meng et al., 2021). The R_{ra} values decreased from 161 ± 82.3 in the NFW episode to 62.2 ± 23.7 in the FW episode (Table 2), indicating that firework emissions lowered particle acidity. As alkaline species, amines showed marked increases in particle count in the FW episode and thus play a key role in governing particle acidity (Chen et al., 2026a; Gui et al., 2025). To improve acidity assessment, amines were incorporated into the calculation scheme, yielding a modified parameter R_{ra}', defined as the ratio of total peak areas of sulfate and nitrate to those of ammonium plus amines (Cheng et al., 2018). After amine inclusion, the revised R_{ra}' dropped to 34.1 ± 12.8 for the FW episode and 29.2 ± 14.9 for the NFW episode, reduced by 1.8 and 5.5 times relative to the original R_{ra}. This finding highlights that amines provide effective buffering against particle acidity, and their inclusion is essential for accurate estimates of particle acidity. The higher R_{ra}' observed in the FW episode further verifies that fireworks emissions drive substantial acid accumulation in particulate matter. Abundant acidic sulfate and nitrate released in the FW episode raised acid burdens, yet the limited buffering capacity of alkaline amines and ammonium could not neutralize excess acidic components and ultimately strengthened particle acidity within firework-influenced air masses. It has been demonstrated that ALWC is primarily regulated by RH and hygroscopic inorganic aerosol components such as ammonium, nitrate, and sulfate (Ali et al., 2023; Chen et al.,

https://doi.org/10.5194/egusphere-2026-6959
Preprint. Discussion started: 20 November 2026
© Author(s) 2026. CC BY 4.0 License.

2026a; Do et al., 2022). Given the elevated RH and higher concentrations of inorganic ions (ammonium, nitrate, and sulfate) during the FW episode (Table 2), ALWC concentrations were substantially higher in the FW episode (1073 ± 287 μg m^{-3}) than in the NFW episode (218 ± 104 μg m^{-3}).

3.2 Elevated imidazole-containing particles driven by firework displays

The 24-h average counts of imidazole-containing particles surged from 4247 in the NFW episode to 9895 in the FW episode, with their fraction among total single particles increasing from 4.7% to 6.6% (Table 1). Simultaneous rises in both the absolute count and relative proportion of imidazole-containing particles suggest substantial inputs from direct firework release and/or accelerated secondary production processes. As shown in Fig. 1a, IM constituted the dominant species of imidazole-containing particles, contributing up to 47.6% in the FW episode and 55.4% in the NFW episode, with EI/DMI/IC (EDI) (32.6% versus 27.8%), MIM (17.9% versus 16.5%), and BM (1.9% versus 0.3%) particles following in decreasing abundance. While their fractional contributions differed between the two episodes, the molecular composition of imidazole-containing particles remained consistent across FW and NFW episodes, suggesting that firework activities altered only the abundance of imidazole-containing particles rather than changing their species distribution. All types of imidazole-containing particles underwent statistically significant increases ($p < 0.01$) in number contributions from the NFW to FW episode, with IM particles showing the most pronounced surge at a 2446 particle count elevation (Table 1). In addition, all imidazole species and total imidazole-containing particles exhibited pronounced diurnal variations, with nighttime counts surpassing daytime values (Fig. 1b). Notably, total count of imidazole-containing particles increased markedly at 21:00 on 21 January and peaked at 02:00 on January 22, coinciding with the episode of the most intensive fireworks burning. Based on these measurements, we conclude that the elevated abundance of imidazole-containing particles in the FW episode is significantly associated with firework emissions.

As shown in Fig. S2, the particle size distribution of imidazole-containing particles in the NFW episode exhibited a bimodal distribution spanning 0.38–0.88 μm, with a primary peak at ~0.56 μm and a secondary peak at ~0.52 μm. In addition, the size distribution broadened to 0.36–0.92 μm and displayed a trimodal pattern in the FW episode, featuring a major peak at ~0.54 μm and secondary peaks at ~0.44 and ~0.62 μm. Such variations are primarily attributable to coupled physical and chemical processes. This phenomenon may stem from extensive internal mixing of imidazole-containing particles with nitrate ($^{46}[NO_2]^-$ and $^{62}[NO_3]^-$) and sulfate ($^{64}[SO_2]^-$ and $^{80}[SO_3]^-$) in the FW episode, whereby intensive incorporation of these inorganic constituents raises the hygroscopic potential of imidazole-containing particles and facilitates subsequent particle growth (Chen et al., 2026a; Wu et al., 2026). Furthermore, ammonium-mediated protonation stabilization and the sulfate salting effect retain imidazoles within the particle phase (Amugoda and Davies, 2025). The mass spectral profile of imidazole-containing particles impacted by firework emissions, obtained by subtracting the spectra acquired in the NFW episode from those collected in the FW episode, revealed a marked enrichment of metal ions (K^+, Na^+, and Mg^{2+}), EC fragments, ammonium, nitrate, and sulfate

https://doi.org/10.5194/egusphere-2026-6959
Preprint. Discussion started: 20 November 2026
© Author(s) 2026. CC BY 4.0 License.

particles (Fig. 1c). Prominent peaks indicative of oxidative aging, including $^{154}[BaO]^+$, $^{59}[C_2H_3O_2]^-$, and $^{73}[C_3H_5O_2]^-$, were also identified in this spectrum.

To evaluate the contribution of firework emissions to imidazole-containing particles, both SPAMS and LC-MS were deployed to resolve the molecular profiles of imidazoles in firework source samples. Unfortunately, no target imidazole signals were detected in either the SPAMS or LC-MS spectra (Figs. 2a, b), demonstrating that imidazoles cannot be directly emitted from firework discharges. Nevertheless, pronounced signals corresponding to organic precursors of imidazoles were clearly identified in the SPAMS mass spectra of firework source samples, including various amines ($^{30}[CH_3NH^+]$, $^{74}([(C_2H_5)_2NH_2]^+)$, and $^{86}([(C_2H_5)_2NCH_2^+])$, Gly ($^{73}[C_2HO_3]^-$), and mGly ($^{71}[C_3H_3O_2]^-$) in the SPAMS mass spectra of firework source samples (Fig. 2b). It can be concluded that the enhanced abundances of imidazole-containing particles in the FW episode largely stem from the secondary formation driven by these firework-released reactive precursors. To further probe the influence of firework emissions on imidazole-containing particles, we focused on the period with intensive firework activity (00:00–04:00 on January 22) and analyzed the hourly variations in both the counts and aging extent of imidazole-containing particles (Fig. 2c). The counts of imidazole-containing particles rose progressively from 00:00 to 2:00, reached a peak at 2:00, and subsequently decreased. To eliminate the confounding effects of atmospheric dilution and transport and better characterize the secondary production of imidazole-containing particles, total imidazole-containing particles are commonly normalized to CO, a well-established tracer for primary combustion emissions, to provide supporting evidence for assessing variations in secondary formation (Meng et al., 2023; Yu et al., 2021). Interestingly, the hourly ratios of total imidazoles/CO followed a consistent temporal pattern that increased gradually from 00:00 to 02:00 and decreased afterwards, further verifying that imidazole-containing particles are predominantly formed via atmospheric secondary processes, rather than being directly emitted from firework displays.

3.3 Impacts of firework displays on the characteristics of imidazole-containing particles

Based on characteristic ionic markers and predominant chemical constituents (presented in Table S3), imidazole-containing particles were classified into eight distinct categories: imidazole-K, imidazole-organic carbon (OC), imidazole-elemental carbon (EC), imidazole-heavy metal (HM), imidazole-mixed elemental-organic carbon (ECOC), imidazole-levoglucosan (LEV), imidazole-dust (DUST), and others (presented in Fig. 3a). In the NFW episode, imidazole-OC (37.1%), imidazole-LEV (20.5%), and imidazole-K (14.4%) constituted the prevailing imidazole particle subtypes and jointly contributed 72.0% to all imidazole-containing particles, with imidazole-HM (13.2%) as the subsequent group. Since OC in wintertime Liaocheng aerosols is predominantly derived from combustion sources (Li et al., 2023), levoglucosan can function as a robust tracer for biomass combustion (Bhattarai et al., 2019). This molecular pattern of imidazole-containing particles in the NFW episode demonstrates that combustion emissions (e.g., biomass burning) govern imidazole abundance instead of secondary formation, consistent with previous findings that imidazoles during dry periods dominantly stem from biomass combustion (Liu et al., 2023). In the FW episode, imidazole-OC still dominated the particle composition, with its fractional contribution rising to

https://doi.org/10.5194/egusphere-2026-6959
Preprint. Discussion started: 20 November 2026
© Author(s) 2026. CC BY 4.0 License.

38.1%. Firework emissions substantially elevated the proportions of imidazole-HM and imidazole-K particles to 22.2% and 20.0%, making them the second- and third- largest contributors in this period. In contrast, daily-averaged particle counts and fractional contributions of imidazole-LEV decreased markedly from 940 and 20.5% in the NFW episode to 469 and 4.7% in the FW episode, reflecting a markedly reduced impact of biomass burning on imidazole-containing particles in the FW episode. While substantial particle loadings originating from firework emissions could passively dilute the fractional contributions of other sources and lower their relative fractions, the synchronous reduction in the absolute count of imidazole-LEV particles further confirms that biomass burning did not drive the rise in imidazole-containing particles observed in the FW episode. These observations verify that the elevated imidazole-containing particles in the FW episode arise mainly from firework discharges instead of biomass burning. It is noteworthy that, aside from imidazole-DUST (5.4%), imidazole-LEV (4.7%), and others (1.1%) representing minor particle fractions, mass spectra of these categories in the FW period consistently exhibited prominent signals of secondary aging species at $^{43}([C_2H_3O]^+)$, $^{59}([C_2H_3O_2]^-)$, and $^{73}([C_3H_5O_2]^-)$, implying that most imidazole-containing particles underwent substantial atmospheric aging.

An adaptive resonance theory neural network algorithm (ART-2a) was applied to enable further categorization of imidazole-containing particles in the FW episode. Following the classification criteria by Huang et al. (2024), eight particle subtypes closely related to firework emissions were identified on the basis of their temporal patterns and mass spectral features: (1) KOC within the OC class, (2) Metal-AlCu and Metal-Ba within the metal class, (3) K-Nit within the K class, (4) EC-NaK-CN, EC-nit-sul, and KEC-CN within the EC class, and (5) ECOC-nit-sul within the ECOC class (Fig. 3b, Table S2). In total, these subtypes accounted for 65.4% of total imidazole-containing particles in the FW episode (Fig. 3c), highlighting fireworks as the predominant driver for the formation of imidazole-containing particles. To explore their mixing characteristics, all imidazole-containing particle types in the FW episode were grouped into FW-related and non-FW categories, and their mixing states were comparatively analyzed (Fig. 3d). The results showed that nitrate exhibited generally higher mixing indices with all imidazole-containing particle types than sulfate, which is associated with the higher atmospheric levels of NO_x relative to SO_2 (Table 1) (Li et al., 2021). The mixing index of the organic fragment (e.g., $C_2H_3O^+$) varied significantly among different types. For FW-related types such as KOC, KEC-CN, Metal-AlCu, and ECOC-nit-sul, the $C_2H_3O^+$ mixing indices were all higher than 0.80, indicating that these particles were highly internally mixed with oxygenated organics and experienced photochemical or aqueous-phase oxidation (Li et al., 2021). In contrast, particle types including K-nit, Metal-Ba, and EC-NaK-CN showed $C_2H_3O^+$ mixing indices below 0.20, with K-LEV as low as 0.01, consistent with their primary emission features. Most FW-related types displayed low mixing indices (< 0.20) with ammonium, whereas their mixing indices with nitrate were mostly higher than 0.88. This pattern suggests that ammonia was not abundant enough to fully neutralize nitric acid and form NH_4NO_3 within firework-dominated particles (Wan et al., 2026). Firework plumes contain abundant metallic elements such as K, Ba, and Ca (Do et al., 2012; Moreno et al., 2007). These metals readily participate in heterogeneous reactions with nitric acid on particle surfaces, which kinetically outcompete the gas-to-particle partitioning of ammonia. As a

https://doi.org/10.5194/egusphere-2026-6959
Preprint. Discussion started: 20 November 2026
© Author(s) 2026. CC BY 4.0 License.

result, nitrate mainly exists in the form of alkali/metal nitrate salts such as KNO_3, $Ba(NO_3)_2$, and $Ca(NO_3)_2$ (Li et al., 2017). Previous studies have demonstrated that Ba and K emitted from fireworks can transform into $Ba(NO_3)_2$ and KNO_3 during atmospheric aging (Lian et al., 2026; Lorenzo et al., 2021). Only a small subset of particle types, such as KOC and ECOC-nit-sul, exhibited relatively high ammonium mixing indices (0.52–0.73). These particles also featured high sulfate mixing indices, indicating that sulfate-rich acidic environments promote ammonium uptake and the internal mixing of ammonium salts (Amugoda and Davies, 2025). These differences in mixing states indicate that firework emissions regulate the chemical composition and aging pathways of imidazole-containing particles via metal competition, acidity regulation, and secondary oxidation, and further control their atmospheric evolution.

3.4 Driving factors of imidazole-containing particles induced by firework displays

3.4.1 Precursor types of imidazole-containing particles

As verified by laboratory experiments, carbonyl species (Gly and mGly) can form imidazoles and other nitrogen heterocycles through nucleophilic reactions when amines or ammonium are present (Chen et al., 2026b; Maxut et al., 2015; Xiao et al., 2025). The average proportions of imidazole-containing particles found within particles that contained amines, ammonium, or carbonyl compounds were 5.0–12.2% in the NFW episode and 7.9–23.1% in the FW episode, which were obviously higher than those in all detected particles in the corresponding episodes (NFW: 4.7%, FW: 6.6%). This observation may suggest that the coexistence of carbonyl compounds and nitrogen-containing species could facilitate imidazole formation. To further investigate the impacts of these precursors on the formation of imidazole-containing particles, ternary diagrams that depict the relative contributions of these three critical precursors in the FW and NFW episodes are displayed in Fig. 4a. In the FW episode, single particles exhibiting a high abundance of imidazoles (hourly count > 700) were predominantly clustered within the compositional range of 26–58% amines, 20–41% carbonyl compounds, and 22–33% ammonium, indicating that the formation of imidazole-containing particles was associated with the coexistence of all three precursors, particularly amines as the indispensable nitrogen donors for imidazole ring formation. The hourly number of imidazole-containing particles in the NFW episode was much lower (< 600), and their precursor compositions were mainly distributed along the carbonyl–amine edge, with ammonium contributing less than ~25%. Additionally, particles with moderate signal intensity of imidazoles (300–600) in the NFW episode exhibited relative contributions of 40–65% amines, 15–50% carbonyl compounds, and merely 5–25% ammonium. These similar patterns indicate that imidazole formation is fundamentally dependent on available amines as nitrogen donors, while sufficient ammonium supply together with carbonyl compounds further facilitates this secondary pathway in the FW episode. As shown in Fig. 4b, ammonium presented no significant correlation with carbonyl compounds ($r = 0.05$, $p > 0.05$), while it exhibited a weak yet significant correlation with imidazole-containing particles ($r = 0.26$, $p < 0.01$) in the NFW episode. Conversely, strong correlations were observed between amines and carbonyl compounds ($r = 0.56$, $p < 0.01$) as well as imidazole-containing particles ($r = 0.61$, $p < 0.01$), confirming the dominant status of amines as nitrogen

https://doi.org/10.5194/egusphere-2026-6959
Preprint. Discussion started: 20 November 2026
© Author(s) 2026. CC BY 4.0 License.

precursor for imidazole generation in the NFW period. In the FW period, imidazole-containing particles were significantly correlated with amines ($r = 0.88$, $p < 0.01$), ammonium ($r = 0.64$, $p < 0.01$), and carbonyl compounds ($r = 0.80$, $p < 0.01$), with the correlation for amines stronger than that for ammonium, indicating that amines still exert a more dominant control on imidazole formation despite the enhanced contribution of ammonium influenced by firework emissions.

Fig. 4c compares the fractions of imidazole-containing particles among different particle mixing types in the two episodes, arising from varied mixing patterns of carbonyl species with ammonium or amines. In the NFW episode, amine–carbonyl mixtures (12.2%) accounted for the largest fraction, followed by ternary precursor mixtures (10.1%) and carbonyl-only particles (9.3%). Although ternary precursor mixtures (23.1%) and amine–carbonyl mixtures (21.5%) remained dominant in the FW episode, ammonium–carbonyl mixtures (14.4%) increased to the third most abundant groups. In both episodes, the fractions of imidazole-containing particles were higher for carbonyl-only particles (NFW: 9.3%, FW: 9.7%) relative to amine-only (NFW: 5.5%, FW: 9.2%) and ammonium-only counterparts (NFW: 5.0%, FW: 7.9%), confirming that carbonyl compounds played a more important role in imidazole formation than amines and ammonium (Kua et al., 2011; Rodriguez et al., 2017; Xu et al., 2025). Meanwhile, the enhanced imidazole formation in the FW episode was closely associated with the synergistic effect between ammonium and amines, largely because carbonyl compounds are more readily converted into imidazole when reacting with mixtures of ammonium and amines than with ammonium or amines individually (Lian et al., 2020). These findings agree with the results of Lian et al. (2021), who demonstrated that extra amines in cloud residual particles could either directly generate additional imidazoles or promote imidazole formation through the synergistic effect between ammonium and amines because carbonyl compounds reacting with mixtures of ammonium and amines produce more imidazole than reactions with ammonium or amines alone. It can be concluded that amines remain the dominant nitrogen source governing this secondary reaction pathway across both observation periods, whereas the synergistic coexistence of amines, ammonium and carbonyl compounds facilitates efficient imidazole production in the FW episode.

3.4.2 Enhanced R_{ra}' promoting imidazole generation induced by fireworks

Computational simulations indicate that acidic environments could facilitate the nucleophilic cyclization reaction between carbonyl compounds and amines, thereby boosting imidazole production in aqueous aerosol particles (Kua et al., 2011). Nevertheless, Yu et al. (2011) documented that the formation rates of condensed-phase imidazoles rose exponentially with elevated pH, implying an ammonium-catalyzed reaction pathway (Yu et al., 2011). Consistent with this finding, Kampf et al. (2012) noted higher yields of bicyclic imidazole species under higher pH conditions (Kampf et al., 2012). On the other hand, field measurements of ambient aerosol samples collected across diverse environments in Europe and China show no correlation between particle pH and imidazole concentrations, even though multiple imidazole species could be detected and quantified in real atmospheric particles. These results appear to be inconsistent with one another, highlighting the need for further investigations to clarify how particulate acidity modulates imidazole formation, particularly in the FW episode (Chen et al.,

https://doi.org/10.5194/egusphere-2026-6959
Preprint. Discussion started: 20 November 2026
© Author(s) 2026. CC BY 4.0 License.

2026b; Teich et al., 2016).

Our previous study has demonstrated that R_{ra}' was significantly correlated with DEA and total amine-containing particles in both FW and NFW episodes, and the enhanced correlations between R_{ra}' and total amine-containing particles in the FW episode suggest that elevated particle acidity could amplify its regulatory effect on the gas-to-particle partitioning of amines (Chen et al., 2026a). As other important precursors of imidazoles, Gly ($r = 0.67$, $p < 0.01$) and mGly ($r = 0.77$, $p < 0.01$) also exhibited positive relationships with R_{ra}' in the FW episode, which were higher than those (Gly: $r = 0.50$, $p < 0.01$; mGly: $r = 0.46$, $p < 0.01$) observed for the NFW episode, indicating that higher particle acidity in the FW episode may favour heterogeneous reactions of Gly and mGly, which are critical for imidazole formation (Fig. S4). Consistent with this inference, field observations and laboratory work have revealed that acid-catalyzed heterogeneous oxidation under acidic aerosol conditions accelerates the uptake and formation of Gly and mGly in the aqueous phase (Jang et al., 2002; Meng et al., 2023; Surratt et al., 2007). Given the enhanced availability of both amine and carbonyl precursors under high-acidity conditions induced by firework emissions, R_{ra}' correlated more strongly with total imidazole-containing particles in the FW episode ($r = 0.51$, $p < 0.01$) relative to the NFW episode ($r = 0.35$, $p < 0.01$). These observations highlight the vital role of particle acidity in promoting the formation of imidazole-containing particles from carbonyl and amine precursors in the FW episode.

3.4.3 RH and ALWC modulation of imidazole formation induced by fireworks

As discussed in Sect. 3.2, the mass spectral profile of imidazole-containing particles influenced by firework emissions was characterized by high intensities of ammonium, metal cations (K^+, Na^+, and Mg^{2+}), nitrate, and sulfate particles (Fig. 1c). Prior studies have demonstrated that inorganic salts (e.g., NH_4NO_3, $(NH_4)_2SO_4$, and Na_2SO_4) released from firework emissions can alter particle hygroscopic properties and reshape the RH dependence of ALWC concentration (Gopinath et al., 2022; Lv et al., 2022; Wu et al., 2018a). Since ALWC is predominantly governed by RH and hygroscopic inorganic aerosols (Shen et al., 2019; Wu et al., 2018b), ALWC exhibited positive correlations with RH in both observation episodes (FW: $r = 0.58$, $p < 0.01$; NFW: $r = 0.72$, $p < 0.01$, Fig. S4). Nevertheless, the RH ranges where ALWC responded sensitively to humidity differed markedly between the two episodes (Fig. 5a). The maximum ALWC growth slope (d_{ALWC}/d_{RH}) occurred in the mid-to-high RH range of 40–80% in the FW episode, while this peak shifted to the lower range of 20–60% in the NFW episode. Furthermore, the absolute ALWC values in the FW episode were substantially higher than those in the NFW episode across all RH intervals. This difference suggests that inorganic salts emitted from firework displays not only elevate the overall hygroscopic growth curve of ambient particles, but may also shift the threshold position of ALWC response to RH.

To explore how RH modulates the formation of imidazole-containing particles, Fig. 5a depicts the variations in the total count of imidazole-containing particles across distinct RH intervals. In the FW episode, the particle count of total imidazoles continuously increased as RH rose from 20% to 80%, with an average count rising by a factor of 2.9. Similarly, the abundance of total imidazoles increased substantially over the RH range of 20–80% for the NFW episode, corresponding to a 1.8-fold

https://doi.org/10.5194/egusphere-2026-6959
Preprint. Discussion started: 20 November 2026
© Author(s) 2026. CC BY 4.0 License.

increase. At RH below 80%, total imidazole-containing particles were positively correlated with RH in both episodes (FW: r = 0.62, p < 0.01; NFW: r = 0.54, p < 0.01; Fig. S4), peaked within the RH range of 60–80%, and declined rapidly once RH exceeded 80%. These results reveal that higher RH promotes the generation of imidazole-containing particles when RH is less than 80%. Interestingly, the average R_{ra}' dropped from 40.4 at 20–80% RH to 21.8 at 80–100% RH in the FW episode (Fig. 5a), which was consistent with the RH dependence of imidazole-containing particles. Comparable variations were also obtained for the NFW episode, where mean R_{ra}' fell from 26.8 for a 20–80% RH range to 20.7 for an 80–100% RH range (Fig. 5a). These observations indicate that the favorable effect of RH weakens at extremely high RH (> 80%), given that excessive RH lowers aerosol acidity, reducing the production of imidazole-containing particles and their precursor species through heterogeneous oxidation driven by aerosol acidity.

The altered hygroscopicity and elevated ALWC driven by firework emissions facilitate the generation of amines and the hydration of carbonyl compounds (Shen et al., 2023; Yu et al., 2011), subsequently triggering nucleophilic reactions that produce imidazole species (Wei et al., 2024; Xu et al., 2025). Consistent with the RH relationship, total imidazole-containing particles were correlated significantly with ALWC when RH remained below 80% for FW (r = 0.65, p < 0.01) and NFW (r = 0.46, p < 0.01) episodes. Still, these robust links weakened across the complete RH range in the FW episode (r = 0.53, p < 0.01) (Fig. S4). This suggests ALWC serves as another factor controlling the generation of imidazole-containing particles, especially for RH less than 80%. At RH below 80 %, higher ALWC concentration supports the dissolution and diffusion of organic precursors (e.g., Gly, mGly, and amines), raises effective collision frequencies, and thus increases R_{ra}' values and favors the production of imidazole species (Xu et al., 2025). However, under excessive RH above 80%, dilution from plentiful ALWC reduces effective reactant concentrations, and larger droplets extend molecular diffusion paths and reduce collision rates, with these combined processes lowering R_{ra}' values and limiting the generation of imidazole-containing particles (Li et al., 2024; Xiao et al., 2025; Xu et al., 2025).

3.4.4 Associations of imidazole formation with inorganic species, O_3, and NO_x

As shown in Table 3, imidazole-containing particles exhibited a slightly higher degree of internal mixing with nitrate (0.93) relative to sulfate (0.91) in the NFW episode, and this discrepancy became more pronounced in the FW episode, with the internal mixing degree of 0.94 for nitrate and 0.80 for sulfate. Specifically, MIM, EDI, and BM showed enhanced internal mixing with nitrate yet a relative reduction in internal mixing with sulfate in the FW episode compared with the NFW episode (Table 3). A previous study has demonstrated that ammonium nitrate features a lower deliquescence relative humidity (DRH) and an effective Henry's law constant equal to or higher than that of ammonium sulfate at RH < 75%, enabling it to more readily take up gaseous precursors (e.g., Gly and mGly) and thereby sustain higher rates of imidazole formation under the same RH conditions (Gen et al., 2018). Correlation analyses revealed slightly stronger correlations of total imidazole-containing particles with sulfate (r = 0.89, p < 0.01) and nitrate (r = 0.89, p < 0.01) in the FW episode compared with the

https://doi.org/10.5194/egusphere-2026-6959
Preprint. Discussion started: 20 November 2026
© Author(s) 2026. CC BY 4.0 License.

corresponding correlations (sulfate: $r = 0.79$, $p < 0.01$; nitrate: $r = 0.80$, $p < 0.01$) in the NFW episode. These findings indicate that elevated particle counts of nitrate and sulfate driven by firework emissions facilitated imidazole formation (Fig. 5b). This finding is consistent with previous reports that nitrate and sulfate can promote imidazole formation (Gen et al., 2018; Li et al., 2017; Lin et al., 2022). Additionally, the degrees of internal mixing of total imidazole-containing particles (0.28) and IM (0.46) in the FW episode with ammonium were substantially higher than those (0.20, 0.25) in the NFW episode, consistent with the ternary diagram results described in Sect. 3.4.1. Similarly, total imidazole-containing particles presented a stronger correlation with ammonium in the FW episode ($r = 0.70$, $p < 0.01$) relative to the NFW episode ($r = 0.26$, $p < 0.01$) (Fig. 4b). This can be explained by the fact that ammonium acts as a key precursor for imidazole formation in the FW episode, and its particle count was 2.6-fold higher in the FW episode than in the NFW episode. This indicates that amines serve as the dominant nitrogen-containing precursor in both FW and NFW episodes, as supported by the strong correlation between imidazole-containing particles and amines in both episodes (NFW: $r = 0.79$, $p < 0.01$; FW: $r = 0.88$, $p < 0.01$), whereas ammonium plays a more important role in imidazole formation in the FW episode relative to the NFW episode. This finding aligns with the results presented in Sect. 3.4.1.

Previous studies have shown that O_3 initiates the photooxidative degradation of imidazole-containing particles through cycloaddition to the C–C double bond on the imidazole ring, producing cyanate, formamide, and formate as end products (Tekle-Röttering et al., 2020). As illustrated in Fig. 5b, imidazole-containing particles exhibited statistically significant anticorrelations with O_3 across the FW ($r = -0.50$, $p < 0.01$) and NFW ($r = -0.60$, $p < 0.01$) campaigns. Such a trend was consistent with the diurnal pattern of imidazole-containing particles, which presented reduced concentrations between 8:00 and 16:00 concurrent with O_3 maxima and vigorous atmospheric photochemical activity (Fig. S5a). Despite this, these negative associations could not be straightforwardly ascribed solely to photodegradation induced by O_3, particularly when daytime and nighttime conditions were differentiated. Throughout the Spring Festival episode, ambient temperatures stayed comparatively low and featured marked diurnal differences (day: 5.5°C, night: 0.01°C), while firework emissions took place mainly after dark. Relative to daytime conditions, diminished solar irradiance and cooler air substantially suppressed photochemical formation of O_3, leading to reduced nighttime O_3 levels. In parallel, the lowered planetary boundary layer (PBL) height overnight (day: 646 m, night: 193 m) limited vertical dispersion and favored near-surface buildup of imidazole-containing particles. Under these meteorological scenarios, substantial firework discharges at night further elevated the counts of imidazole-containing particles. Therefore, depleted nighttime O_3, suppressed PBL height, and strong primary firework emissions contributed to the negative correlation between O_3 and total imidazole-containing particles ($r = -0.58$, $p < 0.01$, Fig. S5b), which cannot be solely ascribed to photodegradation of imidazole-containing particles driven by O_3. Conversely, a pronounced negative correlation was identified between O_3 and total imidazole-containing particles during daytime ($r = -0.44$, $p < 0.05$, Fig. S5b), which featured intense solar irradiance and elevated O_3 levels. PBL trapping and firework discharges exerted negligible impacts on daytime measurements, a finding directly illustrating that intense photodegradation induced by

https://doi.org/10.5194/egusphere-2026-6959
Preprint. Discussion started: 20 November 2026
© Author(s) 2026. CC BY 4.0 License.

O_3 can efficiently deplete imidazole-containing particles, thereby lowering their particle counts in the daytime. This daytime observational evidence aligns with prior field observations that photochemical consumption by O_3 and ·OH radicals represents a major atmospheric sink for imidazole-containing particles under strong solar irradiation conditions (Hu et al., 2022). Elevated NO_x concentrations enhance NO_3· formation and facilitate the production of nitrate via heterogeneous chemical pathways (Brown and Stutz, 2012). As depicted in Fig. S5c, total imidazole-containing particles showed diurnal variations that tracked NO_x concentrations in both FW and NFW episodes, with this pattern especially prominent at night for the FW episode. Consistently, total imidazole-containing particles presented strong relationships with NO_x at night across the two observation episodes, as enhanced nocturnal NO_x concentrations promoted the formation of NO_3· radicals and nitrate, which likely led to the notable rise in the abundance of imidazole-containing particles. Interestingly, such correlation magnitudes were greater in the FW episode ($r = 0.77$, $p < 0.01$) than in the NFW episode ($r = 0.55$, $p < 0.01$) (Fig. S5b), a pattern in agreement with the previously described correlations between imidazole-containing particles and nitrate (FW: $r = 0.89$, $p < 0.01$, NFW: $r = 0.80$, $p < 0.01$) (Fig. 5b). This enhanced correlation can be attributed to the substantial accumulation of NO_x from firework discharge activities, and the accumulated NO_x was rapidly converted into nitrate, which modulated the nighttime formation and buildup of imidazole-containing particles.

3.5 Machine learning attribution of drivers for imidazoles in the FW episode

To overcome the constraints imposed by the limited sample size and multicollinearity among key factors, we constructed six machine learning models covering linear (Ridge, Huber, and PLSR) and nonlinear (GPR, SVR, and GBR) approaches, together with two ensemble strategies (simple averaging and inverse-MSE dynamic weighting). These models were used to simulate total imidazole-containing particles and to enable cross-model comparison, thereby avoiding the limitations of relying on a single model. Details of the complete modeling workflow, hyperparameter configurations, and usability assessment are provided in Text S1, Fig. S6, and Fig. S7. Model performance was evaluated using a rolling-origin (walk-forward) one-step-ahead scheme. Starting from the 20th observation, each model was refitted using all preceding observations and then used to predict the next hour; the resulting predictions therefore constitute out-of-sample estimates. Unless otherwise stated, all R^2, RMSE, and MAE values reported below refer to these walk-forward out-of-sample predictions. Standardized coefficients and permutation importance were obtained from models fitted to the full sample and thus represent in-sample variable importance; they are used for ranking predictors rather than for evaluating predictive performance.

The results of the cross-model comparison show that linear models outperformed their nonlinear counterparts in the FW episode. As shown in Fig. S6a–c, Ridge regression emerged as the best-performing single model (walk-forward $R^2 = 0.86$, RMSE = 57.39, MAE = 44.04), followed by GPR ($R^2 = 0.84$) and Ensemble_New ($R^2 = 0.83$), with GPR capable of generating 95% prediction intervals to quantify time-dependent prediction uncertainty. Huber and PLSR delivered intermediate performance, while nonlinear GBR ($R^2 = 0.68$) and SVR ($R^2 = 0.62$) failed to deliver the anticipated accuracy gains. Segmented diagnostics (Fig. S6f) show that Ridge maintained reasonably high performance in the early ($R^2 = 0.63$) and late ($R^2 = 0.76$)

https://doi.org/10.5194/egusphere-2026-6959
Preprint. Discussion started: 20 November 2026
© Author(s) 2026. CC BY 4.0 License.

portions of the walk-forward prediction period. These results indicate that, within the sampled count range and under walk-forward evaluation, a linear approximation captured most of the variance in total imidazole-containing particles, whereas more complex nonlinear structures were more susceptible to overfitting given the limited sample size. This finding does not negate the potential intrinsic nonlinearity governing imidazole formation, but it shows that linear models provided the most stable predictive performance within the current observational window.

Carbonyl compounds consistently occupied the top position in the permutation importance rankings across all six base models, with mean permutation importance values ranging from 0.086 to 0.195 (Fig. 6d–i). The three linear models yielded stable positive standardized coefficients of 0.22, 0.24, and 0.20 for Ridge, Huber, and PLSR, respectively (Fig. 6a–c), indicating highly consistent effect directions and magnitudes. Amines occupied the second rank in five of the six models and were only outperformed by the temporal variable Hour in the Huber model. Their mean permutation importance ranged from 0.065 to 0.122, and their standardized coefficients in the linear models were all positive, ranging from 0.16 to 0.23 (Fig. 6). This is consistent with the previous discussion identifying carbonyl compounds and amines as critical precursors of imidazole-containing particles in the FW period. Carbonyl compounds and amines were therefore identified as the dominant statistical predictors of imidazole formation in the FW period.

The variable Hour exhibited substantial divergence across models in its contribution. It achieved the highest permutation importance in the Huber model (0.153) (Fig. 6e) but fell to sixth in the GPR and PLSR models, and it showed significant negative standardized coefficients in all linear models. As discussed above, imidazole-containing particles exhibited pronounced diurnal variations driven by multiple physical and meteorological factors, including boundary layer dynamics, firework emission schedules, RH, and solar radiation, rather than arising solely from direct reactive formation. This temporal variability thus exerts complex but substantial controls on imidazole abundance. As a proxy for the acid – base environment of liquid-phase aerosol, R_{ra}' exhibited relatively stable performance across nonlinear models. It ranked third in the Huber, GPR, and SVR models, with permutation importance values of 0.113, 0.075, and 0.062, respectively (Fig. 6e, g and h), and showed positive standardized coefficients in all linear models, with a value of 0.11 in the Huber model (Fig. 6b). The diurnal variation of imidazole concentrations imposed a strong modulating effect on the dataset, while R_{ra}' served as an important secondary predictor of imidazole formation.

Nitrate occupied an intermediate rank in the Ridge and SVR models, yet yielded a permutation importance of 0 in the GBR model, indicating no predictive gain (Fig. 6d, h and i). Ammonium ranked high in the PLSR and SVR models, while its contribution was nearly negligible in the Huber and GPR models. Sulfate, RH, NO_x, and O_3 exerted moderate influences only in selected nonlinear models and weak effects across most other models. These factors may modulate the reaction pathway indirectly by modifying the aerosol acid – base environment and reaction efficiency. In addition, feature multicollinearity may lead to redistribution of permutation importance values among intercorrelated variables. Accordingly, nitrate, ammonium, sulfate, RH, NO_x, and O_3 lacked universally dominant predictive power and are best interpreted as indirect predictors of

https://doi.org/10.5194/egusphere-2026-6959
Preprint. Discussion started: 20 November 2026
© Author(s) 2026. CC BY 4.0 License.

imidazole formation.

ALWC, Sin_Hour, and Cos_Hour had permutation importance values below 0.03 in the vast majority of models, with even negative values in some models, indicating extremely low marginal gains to model performance (Fig. 6d–i). Specifically, ALWC showed permutation importance lower than 0.003 across all linear models and a negative value in the PLSR model (Fig. 6f). These variables offered very limited explanatory power for total imidazole-containing particles in the FW episode and were not key predictors. Therefore, ALWC, Sin_Hour, and Cos_Hour were classified as weak predictors.

Limited by the sample size of valid observations and the use of a single rolling-origin (walk-forward) evaluation, all reported R^2, RMSE, and MAE values quantify out-of-sample predictive performance for this specific FW episode under one sequential partition, rather than demonstrating robust generalizability to other seasons or typical atmospheric pollution scenarios. The standardized coefficients and permutation importance are in-sample variable-importance measures based on full-sample fits and should not be interpreted as causal effects. Even so, building on a chain of evidence derived from comparisons among multiple models, standardized regression coefficients, permutation importance with permutation-sampling uncertainties, and segmented temporal diagnostics on the walk-forward predictions, this study supports a tiered assessment of the predictors governing bulk imidazole concentrations during firework events. It yields physically interpretable and statistically supported, though not causally conclusive, insights into the formation and modulation of imidazole-based secondary aerosol under intense anthropogenic emissions.

4 Summary and conclusions

This study unraveled the molecular distributions, mixing states, and evolutionary mechanisms of imidazole-containing particles associated with firework displays by combining SPAMS observations, source-sample laboratory tests, and multi-model machine-learning analyses. Firework emissions reshaped aerosol physicochemical properties by elevating inorganic salt loadings, ALWC, and R_{ra}', and these changes created aqueous-phase reaction environments conducive to imidazole formation. Source experiments ruled out fireworks as a direct primary source of imidazoles and revealed abundant particulate precursors injected by firework displays, including amines, ammonium, and carbonyl compounds that drove subsequent secondary imidazole production. Compared with the NFW episode, the fractions of imidazole-HM and imidazole-K particles increased substantially, whereas the fraction of biomass-burning-related imidazole-LEV particles decreased; moreover, most imidazole-containing particles in the FW episode exhibited clear signatures of atmospheric aging. Amines served as the dominant nitrogen-containing precursor for imidazole formation in both FW and NFW episodes, whereas ammonium exerted an enhanced contribution to imidazole production in the FW period. Elevated nitrate and sulfate from firework emissions further facilitated imidazole formation through enhanced internal mixing with imidazole-containing particles.

https://doi.org/10.5194/egusphere-2026-6959
Preprint. Discussion started: 20 November 2026
© Author(s) 2026. CC BY 4.0 License.

This work further elucidated the hierarchical modulatory roles of multiple factors for imidazole formation in the FW episode using multi-model machine learning. The integrated hierarchical analysis based on multi-model machine learning revealed that carbonyl compounds and amines were the predominant drivers of imidazole-containing particle formation, whereas R_{ra}' served as a secondary modulatory factor. Sulfate, nitrate, ammonium, RH, and NO_x exhibited strong collinearity, suggesting that their influences were largely indirect. Excessively high RH (> 80%) may suppress imidazole yields by reducing the precursor production via heterogeneous oxidation driven by aerosol acidity, while O_3 serve as a major atmospheric sink for imidazole-containing particles. These findings extend existing knowledge regarding imidazole-related aerosol pollution triggered by firework activities and improve mechanistic understanding of episodic BrC and nitrogen heterocycle aerosol evolution. They also offer critical observational support for atmospheric secondary aerosol modelling and formulating effective firework emission control strategies.

Data availability. The data in this study are available at: https://doi.org/10.5281/zenodo.23994099 (Chen et al., 2026).

Author contribution. JM designed the study. JH, XZ, CW and ZH carried out the experiments. QW, XL and WL performed the data analysis. CC prepared the manuscript with contributions from all co-authors.

Competing interests. The contact author has declared that none of the authors has any competing interests.

Acknowledgments. This work was supported by the National Natural Science Foundation of China (Grant Nos. 42477098, 42607172) and Liaocheng University Doctoral Research Initiation Fund (318-318052403).

References

Ali, U., Faisal, M., Ganguly, D., Kumar, M., and Singh, V.: Analysis of aerosol liquid water content and its role in visibility reduction in Delhi, Science of The Total Environment, 867, 161484, https://doi.org/10.1016/j.scitotenv.2023.161484, 2023.

Amugoda, M. and Davies, J. F.: Ammonium-Induced Stabilization of Imidazoles in Aerosol Particles, ACS Earth Space Chem., 9, 729–737, https://doi.org/10.1021/acsearthspacechem.4c00378, 2025.

Angelino, S., Suess, D. T., and Prather, K. A.: Formation of Aerosol Particles from Reactions of Secondary and Tertiary Alkylamines: Characterization by Aerosol Time-of-Flight Mass Spectrometry, Environ. Sci. Technol., 35, 3130–3138, https://doi.org/10.1021/es0015444, 2001.

Bendersky, M. and Fridkin, S.: The Evolving Landscape of Modern Regression: A Systematic Review and Mapping Study of Penalized, Algorithmic, and Interpretable Models, WIREs Data Min & Knowl, 16, e70078, https://doi.org/10.1002/widm.70078, 2026.

Bhattarai, H., Saikawa, E., Wan, X., Zhu, H., Ram, K., Gao, S., Kang, S., Zhang, Q., Zhang, Y., Wu, G., Wang, X., Kawamura, K., Fu, P., and Cong, Z.: Levoglucosan as a tracer of biomass burning: Recent progress and perspectives, Atmospheric Research, 220, 20–33, https://doi.org/10.1016/j.atmosres.2019.01.004, 2019.

Brown, S. S. and Stutz, J.: Nighttime radical observations and chemistry, Chem. Soc. Rev., 41, 6405, https://doi.org/10.1039/c2cs35181a, 2012.

https://doi.org/10.5194/egusphere-2026-6959
Preprint. Discussion started: 20 November 2026
© Author(s) 2026. CC BY 4.0 License.

Chen, C., Hou, Z., Wang, Q., Liu, F., Hou, J., Wu, C., Li, W., Liu, X., and Meng, J.: Characteristics and gas-particle partitioning of amine-containing particles from firework emissions: New insights from machine learning and single-particle mass spectrometry, Journal of Hazardous Materials, 516, 143446, https://doi.org/10.1016/j.jhazmat.2026.143446, 2026a.

Chen, L., Li, R., Xiao, B., Li, Z., Li, R., Chen, K., Li, R., Zhang, J., Cao, C., Yu, J. Z., Guo, H., and Wang, G.: Atmospheric Nitrogen-Containing Organic Aerosols in Wintertime Sichuan Basin of China: A Key Role of Aqueous-Phase Process in Secondary Production and Optical Absorption, Environmental Science & Technology, 60, 21825–21836, https://doi.org/10.1021/acs.est.6c05422, 2026b.

Chen, M., Meng, J., Li, Y., Wang, Y., Huang, T., Li, Z., Song, X., Wu, C., and Hou, Z.: Effect of COVID-19 lockdown on the characterization and mixing state of carbonaceous particles in the urban atmosphere of Liaocheng, the North China Plain, Particuology, 78, 23–34, https://doi.org/10.1016/j.partic.2022.10.007, 2023.

Cheng, C., Li, M., Chan, C. K., Tong, H., Chen, C., Chen, D., Wu, D., Li, L., Wu, C., Cheng, P., Gao, W., Huang, Z., Li, X., Zhang, Z., Fu, Z., Bi, Y., and Zhou, Z.: Mixing state of oxalic acid containing particles in the rural area of Pearl River Delta, China: implications for the formation mechanism of oxalic acid, Atmos. Chem. Phys., 17, 9519–9533, https://doi.org/10.5194/acp-17-9519-2017, 2017.

Cheng, C., Huang, Z., Chan, C. K., Chu, Y., Li, M., Zhang, T., Ou, Y., Chen, D., Cheng, P., Li, L., Gao, W., Huang, Z., Huang, B., Fu, Z., and Zhou, Z.: Characteristics and mixing state of amine-containing particles at a rural site in the Pearl River Delta, China, Atmos. Chem. Phys., 18, 9147–9159, https://doi.org/10.5194/acp-18-9147-2018, 2018.

De Haan, D. O., Pajunoja, A., Hawkins, L. N., Welsh, H. G., Jimenez, N. G., De Loera, A., Zauscher, M., Andretta, A. D., Joyce, B. W., De Haan, A. C., Riva, M., Cui, T., Surratt, J. D., Cazaunau, M., Formenti, P., Gratien, A., Pangui, E., and Doussin, J.-F.: Methylamine's Effects on Methylglyoxal-Containing Aerosol: Chemical, Physical, and Optical Changes, ACS Earth Space Chem., 3, 1706–1716, https://doi.org/10.1021/acsearthspacechem.9b00103, 2019.

Denkenberger, K. A., Moffet, R. C., Holecek, J. C., Rebotier, T. P., and Prather, K. A.: Real-Time, Single-Particle Measurements of Oligomers in Aged Ambient Aerosol Particles, Environ. Sci. Technol., 41, 5439–5446, https://doi.org/10.1021/es070329l, 2007.

Do, H. D., Lim, Y. B., and Kim, Y. P.: Water uptake and the gas-particle partitioning of nitrate aerosols, Atmos. Chem. Phys. Discuss., 2022, 1–23, https://doi.org/10.5194/acp-2022-364, 2022.

Do, T.-M., Wang, C.-F., Hsieh, Y.-K., and Hsieh, H.-F.: Metals Present in Ambient Air before and after a Firework Festival in Yanshui, Tainan, Taiwan, Aerosol Air Qual. Res., 12, 981–993, https://doi.org/10.4209/aaqr.2012.03.0069, 2012.

Fountoukis, C. and Nenes, A.: ISORROPIA II: a computationally efficient thermodynamic equilibrium model for K^+-Ca^{2+}-Mg^{2+}-NH_4^+-Na^+-SO_4^{2-}-NO^{3-}-Cl^--H_2O aerosols, Atmospheric Chemistry and Physics, 7, 4639–4659, https://doi.org/10.5194/acp-7-4639-2007, 2007.

Friedman, J. H.: Greedy function approximation: A gradient boosting machine, Ann. Statist., 29, 1189–1232, https://doi.org/10.1214/aos/1013203451, 2001.

Gao, K., Zhang, Y., Liu, Y., Yang, M., and Zhu, T.: Screening of imidazoles in atmospheric aerosol particles using a hybrid targeted and untargeted method based on ultra-performance liquid chromatography-quadrupole time-of-flight mass spectrometry, Analytica Chimica Acta, 1163, 338516, https://doi.org/10.1016/j.aca.2021.338516, 2021.

Gen, M., Huang, D. D., and Chan, C. K.: Reactive Uptake of Glyoxal by Ammonium-Containing Salt Particles as a Function of Relative Humidity, Environ. Sci. Technol., 52, 6903–6911, https://doi.org/10.1021/acs.est.8b00606, 2018.

Gopinath, A. K., Raj, S. S., Kommula, S. M., Jose, C., Panda, U., Bishambu, Y., Ojha, N., Ravikrishna, R., Liu, P., and Gunthe, S. S.: Complex Interplay Between Organic and Secondary Inorganic Aerosols With Ambient Relative Humidity Implicates the Aerosol Liquid Water Content Over India During Wintertime, JGR Atmospheres, 127, e2021JD036430,

https://doi.org/10.5194/egusphere-2026-6959
Preprint. Discussion started: 20 November 2026
© Author(s) 2026. CC BY 4.0 License.

https://doi.org/10.1029/2021JD036430, 2022.

Gui, L., Xu, Y., Ma, Y.-J., Yang, T., Xiao, H.-W., Xiao, H., and Xiao, H.-Y.: Firework Display Is a Newly Identified Source of Gaseous and Particulate Amines, Environ. Sci. Technol. Lett., 12, 1387–1393, https://doi.org/10.1021/acs.estlett.5c00806, 2025.

Gündoğdu, S. and Elbir, T.: A Machine Learning Framework Integrating ERA5 Reanalysis for High-Accuracy Reconstruction of Missing Particulate Matter Measurements, Water Air Soil Pollut, 237, 1448, https://doi.org/10.1007/s11270-026-10138-7, 2026.

Hamilton, J. F., Baeza-Romero, M. T., Finessi, E., Rickard, A. R., Healy, R. M., Peppe, S., Adams, T. J., Daniels, M. J. S., Ball, S. M., Goodall, I. C. A., Monks, P. S., Borrás, E., and Muñoz, A.: Online and offline mass spectrometric study of the impact of oxidation and ageing on glyoxal chemistry and uptake onto ammonium sulfate aerosols, Faraday Discuss., 165, 447, https://doi.org/10.1039/c3fd00051f, 2013.

Hu, X., Guo, Z., Sun, W., Lian, X., Fu, Y., Meng, H., Zhu, Y., Zhang, G., Wang, X., Xue, L., Bi, X., Wang, X., and Peng, P.: Atmospheric Processing of Particulate Imidazole Compounds Driven by Photochemistry, Environ. Sci. Technol. Lett., 9, 265–271, https://doi.org/10.1021/acs.estlett.2c00029, 2022.

Huang, X., Ge, Y., Yang, T., Song, Z., Yu, S., Li, Q., Wang, X., Wang, Y., Wang, X., Su, J., Xue, L., Mellouki, A., and Chen, J.: Relaxation of Spring Festival Firework Regulations Leads to a Deterioration in Air Quality, Environ. Sci. Technol., 58, 10185–10194, https://doi.org/10.1021/acs.est.4c00920, 2024.

Huang, Y., Li, L., Li, J., Wang, X., Chen, H., Chen, J., Yang, X., Gross, D. S., Wang, H., Qiao, L., and Chen, C.: A case study of the highly time-resolved evolution of aerosol chemical and optical properties in urban Shanghai, China, Atmos. Chem. Phys., 13, 3931–3944, https://doi.org/10.5194/acp-13-3931-2013, 2013.

Jang, M., Czoschke, N. M., Lee, S., and Kamens, R. M.: Heterogeneous Atmospheric Aerosol Production by Acid-Catalyzed Particle-Phase Reactions, Science, 298, 814–817, https://doi.org/10.1126/science.1075798, 2002.

Juknelevicius, D., Kubilius, R., and Ramanavicius, A.: Oxidizer Ratio and Oxygen Balance Influence on the Emission Spectra of Green-Colored Pyrotechnic Flames, Eur J Inorg Chem, 2015, 5511–5515, https://doi.org/10.1002/ejic.201501128, 2015.

Kampf, C. J., Jakob, R., and Hoffmann, T.: Identification and characterization of aging products in the glyoxal/ammonium sulfate system – implications for light-absorbing material in atmospheric aerosols, Atmos. Chem. Phys., 12, 6323–6333, https://doi.org/10.5194/acp-12-6323-2012, 2012.

Ke, Z., Shao, P., Zhan, C., Wei, C., Liu, Z., Liu, T., and Liu, S.: From clean air to severe haze: evolution of $PM_{2.5}$ and water-soluble ions during a firework-influenced pollution episode, J Atmos Chem, 83, 7, https://doi.org/10.1007/s10874-026-09492-x, 2026.

Klapötke, T. M., Radies, H., Stierstorfer, J., Tarantik, K. R., Chen, G., and Nagori, A.: Coloring Properties of Various High-Nitrogen Compounds in Pyrotechnic Compositions, Propellants Explo Pyrotec, 35, 213–219, https://doi.org/10.1002/prep.201010018, 2010.

Kua, J., Krizner, H. E., and De Haan, D. O.: Thermodynamics and Kinetics of Imidazole Formation from Glyoxal, Methylamine, and Formaldehyde: A Computational Study, J. Phys. Chem. A, 115, 1667–1675, https://doi.org/10.1021/jp111527x, 2011.

Laskin, A., West, C. P., and Hettiyadura, A. P. S.: Molecular insights into the composition, sources, and aging of atmospheric brown carbon, Chem. Soc. Rev., 54, 1583–1612, https://doi.org/10.1039/D3CS00609C, 2025.

Lawrence, S. and Bhathmanabhan, S.: A robust and uncertainty-aware machine learning framework for PM2.5 prediction in a coastal urban Indian environment: implications for sustainable air quality management, Sustain Environ Res, 36, 17, https://doi.org/10.1186/s42834-026-00296-y, 2026.

https://doi.org/10.5194/egusphere-2026-6959
Preprint. Discussion started: 20 November 2026
© Author(s) 2026. CC BY 4.0 License.



Li, J., Xu, T., Lu, X., Chen, H., Nizkorodov, S. A., Chen, J., Yang, X., Mo, Z., Chen, Z., Liu, H., Mao, J., and Liang, G.: Online single particle measurement of fireworks pollution during Chinese New Year in Nanning, Journal of Environmental Sciences, 53, 184–195, https://doi.org/10.1016/j.jes.2016.04.021, 2017.

Li, L.-F., Liu, P., Huang, Q., Zhang, X., Chao, X., Pang, S., Wang, W., Cheng, Y., Su, H., Zhang, Y.-H., and Ge, M.: Rethinking urban haze formation: Atmospheric sulfite conversion rate scales with aerosol surface area, not volume, One Earth, 7, 1082–1095, https://doi.org/10.1016/j.oneear.2024.05.007, 2024.

Li, Y., Chen, M., Wang, Y., Huang, T., Wang, G., Li, Z., Li, J., Meng, J., and Hou, Z.: Seasonal characteristics and provenance of organic aerosols in the urban atmosphere of Liaocheng in the North China Plain: Significant effect of biomass burning, Particuology, 75, 185–198, https://doi.org/10.1016/j.partic.2022.07.012, 2023.

Li, Z., Zhou, R., Wang, Y., Wang, G., Chen, M., Li, Y., Wang, Y., Yi, Y., Hou, Z., Guo, Q., and Meng, J.: Characteristics and sources of amine-containing particles in the urban atmosphere of Liaocheng, a seriously polluted city in North China during the COVID-19 outbreak, Environmental Pollution, 289, 117887, https://doi.org/10.1016/j.envpol.2021.117887, 2021.

Lian, X., Zhang, G., Lin, Q., Liu, F., Peng, L., Yang, Y., Fu, Y., Jiang, F., Bi, X., Chen, D., Wang, X., Peng, P., and Sheng, G.: Seasonal variation of amine-containing particles in urban Guangzhou, China, Atmospheric Environment, 222, 117102, https://doi.org/10.1016/j.atmosenv.2019.117102, 2020.

Lian, X., Zhang, G., Yang, Y., Lin, Q., Fu, Y., Jiang, F., Peng, L., Hu, X., Chen, D., Wang, X., Peng, P., Sheng, G., and Bi, X.: Evidence for the Formation of Imidazole from Carbonyls and Reduced Nitrogen Species at the Individual Particle Level in the Ambient Atmosphere, Environ. Sci. Technol. Lett., 8, 9–15, https://doi.org/10.1021/acs.estlett.0c00722, 2021.

Lian, X., Pei, C., Sun, W., Lv, C., Huang, K., Lei, L., Huang, B., Cheng, C., Zhang, G., Bi, X., Zhou, Z., and Li, M.: Evolution of firework-related barium aerosols: insights from single-particle analysis and mass concentration monitoring, EGUsphere, 2026, 1–24, https://doi.org/10.5194/egusphere-2026-1853, 2026.

Lin, C.-C.: A review of the impact of fireworks on particulate matter in ambient air, Journal of the Air & Waste Management Association, 66, 1171–1182, https://doi.org/10.1080/10962247.2016.1219280, 2016.

Lin, P., Laskin, J., Nizkorodov, S. A., and Laskin, A.: Revealing Brown Carbon Chromophores Produced in Reactions of Methylglyoxal with Ammonium Sulfate, Environ. Sci. Technol., 49, 14257–14266, https://doi.org/10.1021/acs.est.5b03608, 2015.

Lin, X., Huang, M., Lu, T., Zhao, W., Hu, C., Gu, X., and Zhang, W.: Characterization of Imidazole Compounds in Aqueous Secondary Organic Aerosol Generated from Evaporation of Droplets Containing Pyruvaldehyde and Inorganic Ammonium, Atmosphere, 13, 970, https://doi.org/10.3390/atmos13060970, 2022.

Liu, L., Li, W., Tang, S., Alam, M. S., Crilley, L. R., Srivastava, D., Khare, M., Moreno, N., Bloss, W. J., and Shi, Z.: Microscopic Insights into Firework- and Biomass-Burning-Derived Haze Particles during the Diwali Festival in Delhi, India, Environ. Sci. Technol., 60, 6454–6463, https://doi.org/10.1021/acs.est.5c16031, 2026.

Liu, X., Wang, H., Wang, F., Lv, S., Wu, C., Zhao, Y., Zhang, S., Liu, S., Xu, X., Lei, Y., and Wang, G.: Secondary Formation of Atmospheric Brown Carbon in China Haze: Implication for an Enhancing Role of Ammonia, Environ. Sci. Technol., 57, 11163–11172, https://doi.org/10.1021/acs.est.3c03948, 2023.

Lorenzo, G. R., Bañaga, P. A., Cambaliza, M. O., Cruz, M. T., AzadiAghdam, M., Arellano, A., Betito, G., Braun, R., Corral, A. F., Dadashazar, H., Edwards, E.-L., Eloranta, E., Holz, R., Leung, G., Ma, L., MacDonald, A. B., Reid, J. S., Simpas, J. B., Stahl, C., Visaga, S. M., and Sorooshian, A.: Measurement report: Firework impacts on air quality in Metro Manila, Philippines, during the 2019 New Year revelry, Atmos. Chem. Phys., 21, 6155–6173, https://doi.org/10.5194/acp-21-6155-2021, 2021.

https://doi.org/10.5194/egusphere-2026-6959
Preprint. Discussion started: 20 November 2026
© Author(s) 2026. CC BY 4.0 License.

Lv, S., Wang, F., Wu, C., Chen, Y., Liu, S., Zhang, S., Li, D., Du, W., Zhang, F., Wang, H., Huang, C., Fu, Q., Duan, Y., and Wang, G.: Gas-to-Aerosol Phase Partitioning of Atmospheric Water-Soluble Organic Compounds at a Rural Site in China: An Enhancing Effect of NH3 on SOA Formation, Environ. Sci. Technol., 56, 3915–3924, https://doi.org/10.1021/acs.est.1c06855, 2022.

Ma, J., Meng, J., Wang, Y., Liu, X., Zhang, X., Yang, K., Liu, Q., and Hou, Z.: Mixing state and evolutionary mechanism of oxalic acid homologs in Liaocheng, East China: Insights from seasonal and hourly observations, Particuology, 95, 223–234, https://doi.org/10.1016/j.partic.2024.09.011, 2024.

Maxut, A., Nozière, B., Fenet, B., and Mechakra, H.: Formation mechanisms and yields of small imidazoles from reactions of glyoxal with NH4+ in water at neutral pH, Phys. Chem. Chem. Phys., 17, 20416–20424, https://doi.org/10.1039/C5CP03113C, 2015.

Meng, J., Li, Z., Zhou, R., Chen, M., Li, Y., Yi, Y., Ding, Z., Li, H., Yan, L., Hou, Z., and Wang, G.: Enhanced photochemical formation of secondary organic aerosols during the COVID-19 lockdown in Northern China, Science of The Total Environment, 758, 143709, https://doi.org/10.1016/j.scitotenv.2020.143709, 2021.

Meng, J., Wang, Y., Li, Y., Huang, T., Wang, Z., Wang, Y., Chen, M., Hou, Z., Zhou, H., Lu, K., Kawamura, K., and Fu, P.: Measurement Report: Investigation on the sources and formation processes of dicarboxylic acids and related species in urban aerosols before and during the COVID-19 lockdown in Jinan, East China, Atmos. Chem. Phys., 23, 14481–14503, https://doi.org/10.5194/acp-23-14481-2023, 2023.

Moreno, T., Querol, X., Alastuey, A., Cruz Minguillón, M., Pey, J., Rodriguez, S., Vicente Miró, J., Felis, C., and Gibbons, W.: Recreational atmospheric pollution episodes: Inhalable metalliferous particles from firework displays, Atmospheric Environment, 41, 913–922, https://doi.org/10.1016/j.atmosenv.2006.09.019, 2007.

Naslidnyk, M., Kanagawa, M., Karvonen, T., and Mahsereci, M.: Comparing Scale Parameter Estimators for Gaussian Process Interpolation with the Brownian Motion Prior: Leave-One-Out Cross Validation and Maximum Likelihood, SIAM/ASA J. Uncertainty Quantification, 13, 679–717, https://doi.org/10.1137/23M1586884, 2025.

Ouyang, D., Yang, C., Zhang, Q., Yan, H., and Pang, W.: Effect of metal oxides on the light radiation intensity of Ba(NO3)2/Mg-containing pyrotechnic mixtures combustion, Sci Rep, 12, 19522, https://doi.org/10.1038/s41598-022-22858-x, 2022.

Powelson, M. H., Espelien, B. M., Hawkins, L. N., Galloway, M. M., and De Haan, D. O.: Brown Carbon Formation by Aqueous-Phase Carbonyl Compound Reactions with Amines and Ammonium Sulfate, Environ. Sci. Technol., 48, 985–993, https://doi.org/10.1021/es4038325, 2014.

Ravikumar, A., Periyasamy, V., Devi, K. M. K., Krishnamoorthy, R. G., and Mariavalavan, O. K.: A hybrid SERWI ensemble model for crop yield prediction using an inverse RMSE weighting strategy, Sci Rep, 15, 45085, https://doi.org/10.1038/s41598-025-31987-y, 2025.

Robinson, E. S., Saleh, R., and Donahue, N. M.: Organic Aerosol Mixing Observed by Single-Particle Mass Spectrometry, J. Phys. Chem. A, 117, 13935–13945, https://doi.org/10.1021/jp405789t, 2013.

Rodriguez, A. A., de Loera, A., Powelson, M. H., Galloway, M. M., and De Haan, D. O.: Formaldehyde and Acetaldehyde Increase Aqueous-Phase Production of Imidazoles in Methylglyoxal/Amine Mixtures: Quantifying a Secondary Organic Aerosol Formation Mechanism, Environmental Science & Technology Letters, 4, 234–239, https://doi.org/10.1021/acs.estlett.7b00129, 2017.

Sabatini, J. J., Koch, E., Poret, J. C., Moretti, J. D., and Harbol, S. M.: Chlorine-Free Red-Burning Pyrotechnics, Angew Chem Int Ed, 54, 10968–10970, https://doi.org/10.1002/anie.201505829, 2015.

Shen, M., Qi, W., Liu, Y., Zhang, Y., Dai, W., Li, L., Guo, X., Cao, Y., Jiang, Y., Wang, Q., Li, S., Wang, Q., and Li, J.: Measurement report: Observational insights into the impact of dust transport on atmospheric dicarboxylic acids in ground region and free

https://doi.org/10.5194/egusphere-2026-6959
Preprint. Discussion started: 20 November 2026
© Author(s) 2026. CC BY 4.0 License.

troposphere, Atmos. Chem. Phys., 25, 16147–16165, https://doi.org/10.5194/acp-25-16147-2025, 2025.

Shen, X., Chen, J., Li, G., and An, T.: A new advance in the pollution profile, transformation process, and contribution to aerosol formation and aging of atmospheric amines, Environ. Sci.: Atmos., 3, 444–473, https://doi.org/10.1039/D2EA00167E, 2023.

Shen, X. J., Sun, J. Y., Zhang, X. Y., Zhang, Y. M., Zhong, J. T., Wang, X., Wang, Y. Q., and Xia, C.: Variations in submicron aerosol liquid water content and the contribution of chemical components during heavy aerosol pollution episodes in winter in Beijing, Science of The Total Environment, 693, 133521, https://doi.org/10.1016/j.scitotenv.2019.07.327, 2019.

Smola, A. J. and Schölkopf, B.: A tutorial on support vector regression, Statistics and Computing, 14, 199–222, https://doi.org/10.1023/B:STCO.0000035301.49549.88, 2004.

Steinhauser, G. and Klapötke, T. M.: "Green" Pyrotechnics: A Chemists' Challenge, Angew Chem Int Ed, 47, 3330–3347, https://doi.org/10.1002/anie.200704510, 2008.

Stock, J. H. and Watson, M. W.: Combination forecasts of output growth in a seven-country data set, Journal of Forecasting, 23, 405–430, https://doi.org/10.1002/for.928, 2004.

Surratt, J. D., Lewandowski, M., Offenberg, J. H., Jaoui, M., Kleindienst, T. E., Edney, E. O., and Seinfeld, J. H.: Effect of Acidity on Secondary Organic Aerosol Formation from Isoprene, Environ. Sci. Technol., 41, 5363–5369, https://doi.org/10.1021/es0704176, 2007.

Tang, M., Ji, D.-S., Gao, W.-K., Yu, Z.-W., Chen, K., and Cao, W.: Characteristics of air quality in Tianjin during the Spring Festival period of 2015, Atmospheric and Oceanic Science Letters, 9, 15–21, https://doi.org/10.1080/16742834.2015.1131948, 2016.

Teich, M., Van Pinxteren, D., Kecorius, S., Wang, Z., and Herrmann, H.: First Quantification of Imidazoles in Ambient Aerosol Particles: Potential Photosensitizers, Brown Carbon Constituents, and Hazardous Components, Environ. Sci. Technol., 50, 1166–1173, https://doi.org/10.1021/acs.est.5b05474, 2016.

Tekle-Röttering, A., Lim, S., Reisz, E., Lutze, H. V., Abdighahroudi, M. S., Willach, S., Schmidt, W., Tentscher, P. R., Rentsch, D., McArdell, C. S., Schmidt, T. C., and Von Gunten, U.: Reactions of pyrrole, imidazole, and pyrazole with ozone: kinetics and mechanisms, Environ. Sci.: Water Res. Technol., 6, 976–992, https://doi.org/10.1039/C9EW01078E, 2020.

Tinel, L., Dumas, S., and George, C.: A time-resolved study of the multiphase chemistry of excited carbonyls: Imidazole-2-carboxaldehyde and halides, Comptes Rendus. Chimie, 17, 801–807, https://doi.org/10.1016/j.crci.2014.03.008, 2014.

Tripathi, S., Chakraborty, A., Parkar, V., and Mahant, M.: Stark variations in the impacts of Diwali fireworks on aerosol characteristics and aging: Influence of festival timing, meteorology, transport and emissions, Atmospheric Environment, 379, 122069, https://doi.org/10.1016/j.atmosenv.2026.122069, 2026.

Wan, R., Zheng, G., Li, Y., Duan, X., Jiang, J., and He, K.: Driving factors for the activity coefficient of atmospheric ammonium nitrate: discrepancies among thermodynamic models and impact on nitrate pollutions, Atmos. Chem. Phys., 26, 1795–1807, https://doi.org/10.5194/acp-26-1795-2026, 2026.

Wei, B., Zhang, R., Sit, P. H.-L., He, M., and Chan, C. K.: Formation and Oxidation of Imidazole in Tropospheric Aqueous-Phase Chemistry: A Computational Study, ACS EST Air, 1, 617–627, https://doi.org/10.1021/acsestair.3c00097, 2024.

Wold, S., Sjöström, M., and Eriksson, L.: PLS-regression: a basic tool of chemometrics, Chemometrics and Intelligent Laboratory Systems, 58, 109–130, https://doi.org/10.1016/S0169-7439(01)00155-1, 2001.

Wu, C., Wang, G., Wang, J., Li, J., Ren, Y., Zhang, L., Cao, C., Li, J., Ge, S., Xie, Y., Wang, X., and Xue, G.: Chemical characteristics of

https://doi.org/10.5194/egusphere-2026-6959
Preprint. Discussion started: 20 November 2026
© Author(s) 2026. CC BY 4.0 License.

haze particles in Xi'an during Chinese Spring Festival: Impact of fireworks burning, Journal of Environmental Sciences, 71, 179–187, https://doi.org/10.1016/j.jes.2018.04.008, 2018a.

Wu, T., Lin, M., Zheng, R., Zhang, K., Niu, X., and Zhou, J.: Hygroscopic growth kinetics and microscopic mechanisms of various inorganic salt nanoparticles: A molecular dynamics study, Advanced Powder Technology, 37, 105398, https://doi.org/10.1016/j.apt.2026.105398, 2026.

Wu, Z., Wang, Y., Tan, T., Zhu, Y., Li, M., Shang, D., Wang, H., Lu, K., Guo, S., Zeng, L., and Zhang, Y.: Aerosol Liquid Water Driven by Anthropogenic Inorganic Salts: Implying Its Key Role in Haze Formation over the North China Plain, Environ. Sci. Technol. Lett., 5, 160–166, https://doi.org/10.1021/acs.estlett.8b00021, 2018b.

Xiao, B., Wang, G., Li, Z., Li, R., Liang, C., Wang, H., Zhang, S., Wu, C., Li, R., Zhang, F., Zhang, R., Wu, Y., and Zhang, L.: High Contribution of Secondary Formation to Brown Carbon in China Humid Haze: Enhancing Role of Ammonia and Amines, Environ. Sci. Technol., 59, 27530–27540, https://doi.org/10.1021/acs.est.5c13436, 2025.

Xu, H., Sun, T., Wang, Y., Wang, L., Chen, L., Gao, X., and Cen, K.: Atmospheric imidazole formation: Unraveling the roles of precursors, humidity, and aerosol acidity, Environmental Pollution, 386, 127214, https://doi.org/10.1016/j.envpol.2025.127214, 2025.

Yu, G., Bayer, A. R., Galloway, M. M., Korshavn, K. J., Fry, C. G., and Keutsch, F. N.: Glyoxal in Aqueous Ammonium Sulfate Solutions: Products, Kinetics and Hydration Effects, Environ. Sci. Technol., 45, 6336–6342, https://doi.org/10.1021/es200989n, 2011.

Yu, Q., Chen, J., Cheng, S., Qin, W., Zhang, Y., Sun, Y., and Ahmad, M.: Seasonal variation of dicarboxylic acids in PM2.5 in Beijing: Implications for the formation and aging processes of secondary organic aerosols, Science of The Total Environment, 763, 142964, https://doi.org/10.1016/j.scitotenv.2020.142964, 2021.

Zauscher, M. D., Wang, Y., Moore, M. J. K., Gaston, C. J., and Prather, K. A.: Air Quality Impact and Physicochemical Aging of Biomass Burning Aerosols during the 2007 San Diego Wildfires, Environ. Sci. Technol., 47, 7633–7643, https://doi.org/10.1021/es4004137, 2013.

Zhu, M., Huang, M., Lu, T., Cai, S., Shan, X., Sheng, L., Zhao, W., Gu, X., and Zhang, W.: Experimental study on the imidazoles of aqueous secondary organic aerosol formed from reaction of methylglyoxal and ammonium sulphate, Atmospheric Pollution Research, 13, 101535, https://doi.org/10.1016/j.apr.2022.101535, 2022.

https://doi.org/10.5194/egusphere-2026-6959
Preprint. Discussion started: 20 November 2026
© Author(s) 2026. CC BY 4.0 License.

Table captions

Table 1. Tracer ions, particle counts, and relative fractions of distinct imidazole-containing particles among total imidazoles during the non-firework (NFW) and firework (FW) episodes.

Table 2. Meteorological factors, gaseous pollutants, inorganic ions, relative aerosol acidity (R_{ra}), aerosol liquid water content (ALWC), precursors of imidazole-containing particles, and other species during the NFW and FW episodes in Liaocheng.

Table 3. Mixing states of total imidazole-containing particles and individual subtypes with sulfate, nitrate, and ammonium during the NFW and FW episodes.

Figure captions

Figure 1. (a) Comparison of molecular compositions of imidazole-containing particles between NFW and FW episodes; (b) diurnal patterns in total imidazole-containing particles and individual subtypes during the NFW and FW episodes; (c) differential spectra of imidazole-containing particles calculated by subtracting NFW signals from FW signals.

Figure 2. (a) Retention time and mass information of imidazoles from five standard solutions (including imidazole-2-carboxaldehyde (IC), 2,2′-biimidazole (BM), 2-ethylimidazole (EI), 2,4-dimethylimidazole (DMI), and 4-methylimidazole (MIM)) and forty firework source samples determined by high-performance liquid chromatography (HPLC) coupled to an Orbitrap mass spectrometer; (b) mass spectra of imidazole-containing particles from five standard solutions and forty firework source samples using a single-particle aerosol mass spectrometer (SPAMS); (c) hourly variations in the count of total imidazole-containing particles and the ratio of total imidazoles to CO in the FW episode.

Figure 3. (a) Differences in imidazole-containing particle types between NFW and FW episodes; (b) proportions of distinct imidazole-containing particle subtypes in the FW episode; (c) proportions of firework-related classified subtypes in total imidazole-containing particles from ambient particles; (d) heatmap of the mixing states between individual imidazole compounds and $C_2H_3O^+$, NH_4^+, HSO_4^-, and NO_3^-.

Figure 4. (a) Ternary diagram of imidazole precursors (carbonyl compounds, amines, and ammonium) during the FW and NFW episodes; (b) heatmap of the mixing states of total imidazole-containing particles with three precursors (including carbonyl compounds, amines, and ammonium); (c) number fractions of total imidazoles in each particle type during the FW and NFW episodes.

Figure 5. (a) Variations in aerosol liquid water content (ALWC), relative aerosol acidity (R_{ra}), modified relative aerosol acidity (R_{ra}'), and total imidazoles under varied relative humidity (RH) conditions during FW and NFW episodes; (b) correlation of nitrate, sulfate, and total imidazole-containing particles with R_{ra}', RH, ALWC and NO_x concentrations during the NFW and FW periods.

Figure 6. Comparison of feature importance for predictors of total imidazole-containing particles under logarithmic transformation. Standardized regression coefficients of 13 predictors in three linear models correspond to (a) Ridge, (b) Huber, and (c) PLSR, where bar length and direction represent the magnitude and sign of each variable's independent effect; (d–i) mean permutation importance of predictors from six base models correspond to (d) Ridge, (e) Huber, (f) PLSR, (g) GPR, (h) SVR, and (i) GBR. Error bars denote the standard deviation from repeated permutation sampling. All features are ranked by overall predictive contribution.

https://doi.org/10.5194/egusphere-2026-6959
Preprint. Discussion started: 20 November 2026
© Author(s) 2026. CC BY 4.0 License.

Table 1. Tracer ions, particle counts, and relative fractions of distinct imidazole-containing particles among total imidazoles during the non-firework (NFW) and firework (FW) episodes.

Tracer ion	*m/z*	Species	NFW		FW		Increase
			Count	Percentage	Count	Percentage	count
$(C_3H_4N_2+H)^+$	69	IM	3032	55.4%	5478	47.6%	2446
$(C_4H_5N_2)^+$	81	MIM	903	16.5%	2050	17.9%	1147
$(C_5H_8N_2+H)^+$/ $(C_4H_4N_2O+H)^+$	97	EI/DMI/IC(EDI)	1518	27.8%	3734	32.6%	2216
$(C_6H_6N_4)^+$	134	BM	18	0.3%	221	1.9%	203
		Total imidazoles	4247	4.7% [a]	9895	6.6%	5648

[a] Relative abundances of imidazole-containing particles in total single particles.

845

https://doi.org/10.5194/egusphere-2026-6959
Preprint. Discussion started: 20 November 2026
© Author(s) 2026. CC BY 4.0 License.

Table 2. Meteorological factors, gaseous pollutants, inorganic ions, relative aerosol acidity (R_{ra}), aerosol liquid water content (ALWC), precursors of imidazole-containing particles, and other species during the NFW and FW episodes in Liaocheng.

Parameters	NFW	FW
I. Meteorological parameters		
Temperature (ºC)	-0.3 ± 5.4 (-12.5–15.1)	2.7 ± 3.8 (-2.7–9.4)
Relative humidity (%)	39.2 ± 15.6 (12.7–90.1)	57.6 ± 21.8 (21.1–96.3)
Solar radiation (W m^{-2})	5.2 ± 8.0 (0.0–27.4)	3.6 ± 5.5 (0.0–17.3)
Wind speed (m s^{-1})	4.2 ± 2.3 (0.8–11.0)	4.3 ± 3.8 (0.8–14.1)
Planetary boundary layer height (m)	417 ± 479 (10.7–1864)	419 ± 467 (15.8–1543)
II. Gaseous pollutants and inorganic ions (μg m^{-3})		
SO_2	7.2 ± 5.0 (1.0–26.0)	15.9 ± 10.3 (3.0–45.0)
CO	900 ± 264 (200–1700)	1500 ± 268 (800–1900)
O_3	50.4 ± 22.2 (4.0–118)	50.4 ± 23.7 (11.0–113)
NO_x	34.8 ± 29.4 (7.0–248)	29.9 ± 7.7 (13.0–47.0)
NH_4^+	4.1 ± 2.4 (0.0–10.5)	16.0 ± 3.5 (7.4–23.2)
SO_4^{2-}	4.8 ± 2.0 (1.7–11.7)	24.1 ± 8.3 (9.6–41.6)
NO_3^-	10.9 ± 3.7 (4.0–25.5)	33.1 ± 6.9 (13.3–43.2)
III. Particle counts of chemical species using a single-particle aerosol mass spectrometer		
Ammonium	489 ± 438 (38–2242)	1280 ± 256 (745–2113)
Sulfate	3258 ± 1970 (424–9949)	4912 ± 1659 (1736–7479)
Nitrate	3463 ± 2143 (391–10113)	5956 ± 1767 (1880–8744)
Levoglucosan	276 ± 189 (25.0–1035)	188 ± 120 (3.0–423)
Amines	833 ± 435 (164–2110)	1581 ± 1142 (241–4018)
Glyoxal	409 ± 238 (37.0–1421)	690 ± 550 (17.0–2219)
Methylglyoxal	988 ± 484 (129–2451)	2530 ± 1828 (236–7567)
Cl	1149 ± 638 (116–2958)	4345 ± 2572 (479–10885)
Cu	1430 ± 954 (309–7095)	2109 ± 1049 (536–4474)
Ba	9.8 ± 11.4 (0.0–82.0)	123 ± 59.0 (45.0–292)
Sr	3.0 ± 2.8 (0.0–13.0)	31.2 ± 20.5 (3.0–81.0)
IV. Other species		
$PM_{2.5}$ (μg m^{-3})	43.7 ± 24.3 (3.0–101)	192 ± 71.1 (36.0–343)
PM_{10} (μg m^{-3})	94.8 ± 50.5 (21.0–250)	220 ± 102 (154–596)
R_{ra}	161 ± 82.3 (33.1–406)	62.2 ± 23.7 (25.9–105)
R_{ra}'	29.2 ± 14.9 (6.0–73.4)	34.1 ± 12.8 (14.0–57.2)
ALWC (μg m^{-3})	218 ± 104 (24.1–576)	1073 ± 287 (339–1624)

https://doi.org/10.5194/egusphere-2026-6959
Preprint. Discussion started: 20 November 2026
© Author(s) 2026. CC BY 4.0 License.

Table 3. Mixing states of total imidazole-containing particles and individual subtypes with sulfate, nitrate, and ammonium during the NFW and FW episodes.

Species	NFW			FW		
	Sulfate	Nitrate	Ammonium	Sulfate	Nitrate	Ammonium
Total imidazoles	0.91	0.93	0.20	0.80	0.94	0.28
IM	0.99	0.94	0.25	0.99	0.94	0.46
MIM	0.81	0.89	0.14	0.72	0.92	0.16
EDI	0.83	0.91	0.14	0.63	0.92	0.10
BM	0.42	0.83	0.23	0.28	0.93	0.05

https://doi.org/10.5194/egusphere-2026-6959
Preprint. Discussion started: 20 November 2026
© Author(s) 2026. CC BY 4.0 License.

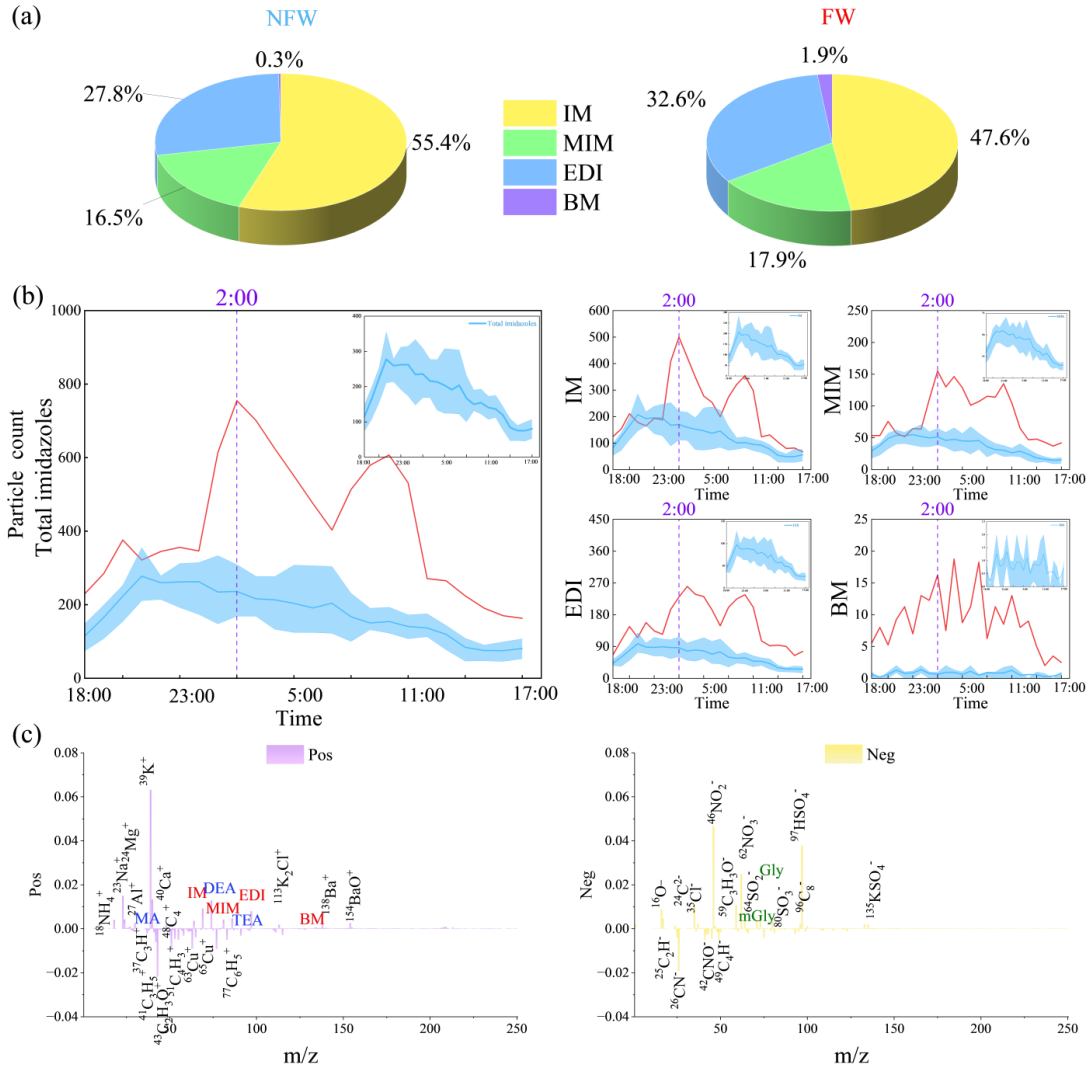


Figure 1. (a) Comparison of molecular compositions of imidazole-containing particles between NFW and FW episodes; (b) diurnal patterns in total imidazole-containing particles and individual subtypes during the NFW and FW episodes; (c) differential spectra of imidazole-containing particles calculated by subtracting NFW signals from FW signals.

https://doi.org/10.5194/egusphere-2026-6959
Preprint. Discussion started: 20 November 2026
© Author(s) 2026. CC BY 4.0 License.

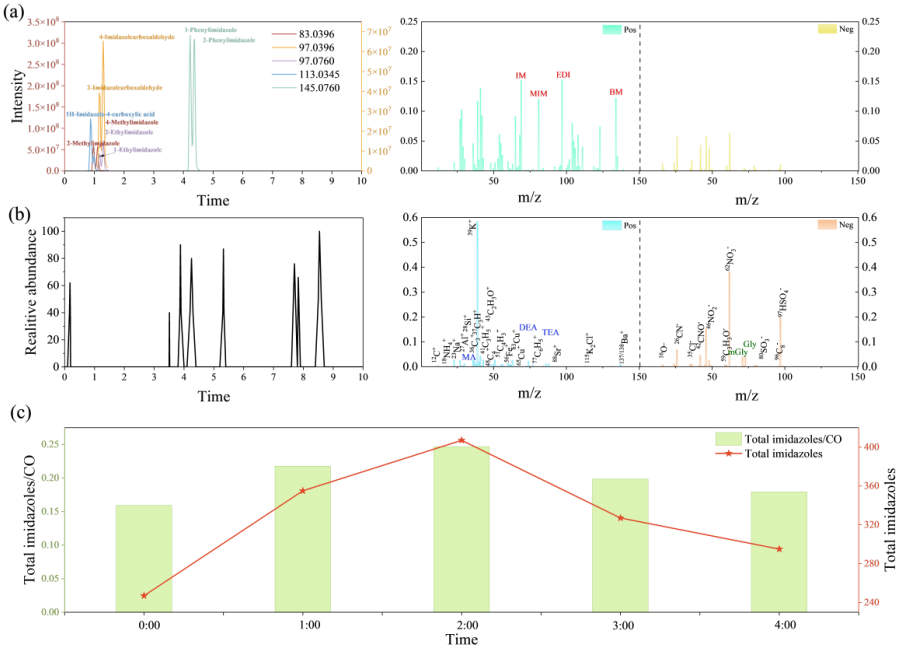


Figure 2. (a) Retention time and mass information of imidazoles from five standard solutions (including imidazole-2-carboxaldehyde (IC), 2,2′-biimidazole (BM), 2-ethylimidazole (EI), 2,4-dimethylimidazole (DMI), and 4-methylimidazole (MIM)) and forty firework source samples determined by high-performance liquid chromatography (HPLC) coupled to an Orbitrap mass spectrometer; (b) mass spectra of imidazole-containing particles from five standard solutions and forty firework source samples using a single-particle aerosol mass spectrometer (SPAMS); (c) hourly variations in the count of total imidazole-containing particles and the ratio of total imidazoles to CO in the FW episode.

https://doi.org/10.5194/egusphere-2026-6959
Preprint. Discussion started: 20 November 2026
© Author(s) 2026. CC BY 4.0 License.

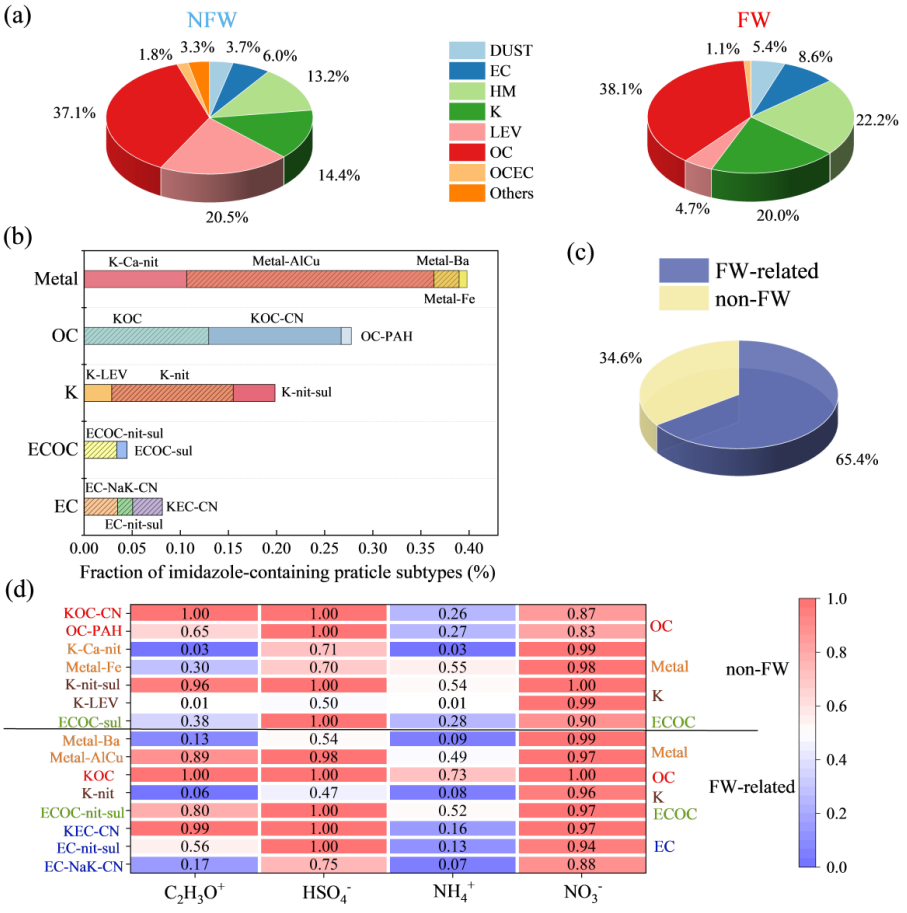


Figure 3. (a) Differences in imidazole-containing particle types between NFW and FW episodes; (b) proportions of distinct imidazole-containing particle subtypes in the FW episode; (c) proportions of firework-related classified subtypes in total imidazole-containing particles from ambient particles; (d) heatmap of the mixing states between individual imidazole compounds and $C_2H_3O^+$, NH_4^+, HSO_4^-, and NO_3^-.

https://doi.org/10.5194/egusphere-2026-6959
Preprint. Discussion started: 20 November 2026
© Author(s) 2026. CC BY 4.0 License.

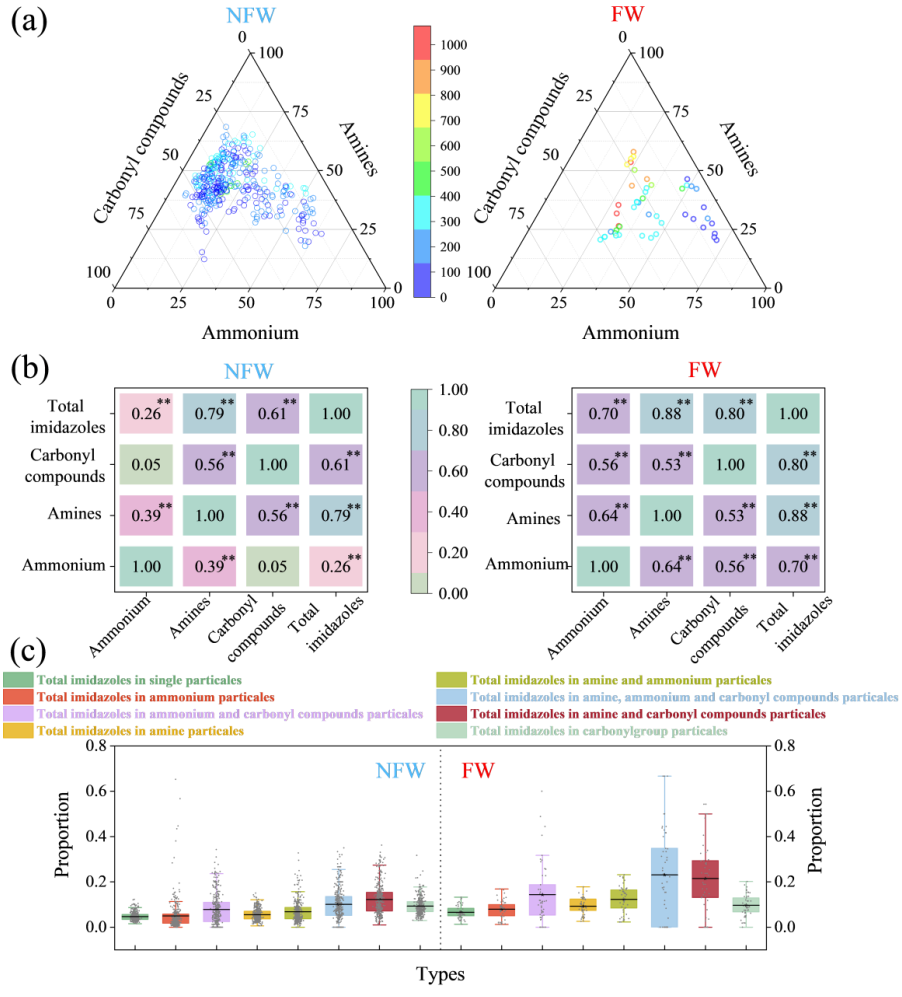


Figure 4. (a) Ternary diagram of imidazole precursors (carbonyl compounds, amines, and ammonium) during the FW and NFW episodes; (b) heatmap of the mixing states of total imidazole-containing particles with three precursors (including carbonyl compounds, amines, and ammonium); (c) number fractions of total imidazoles in each particle type during the FW and NFW episodes.

https://doi.org/10.5194/egusphere-2026-6959
Preprint. Discussion started: 20 November 2026
© Author(s) 2026. CC BY 4.0 License.

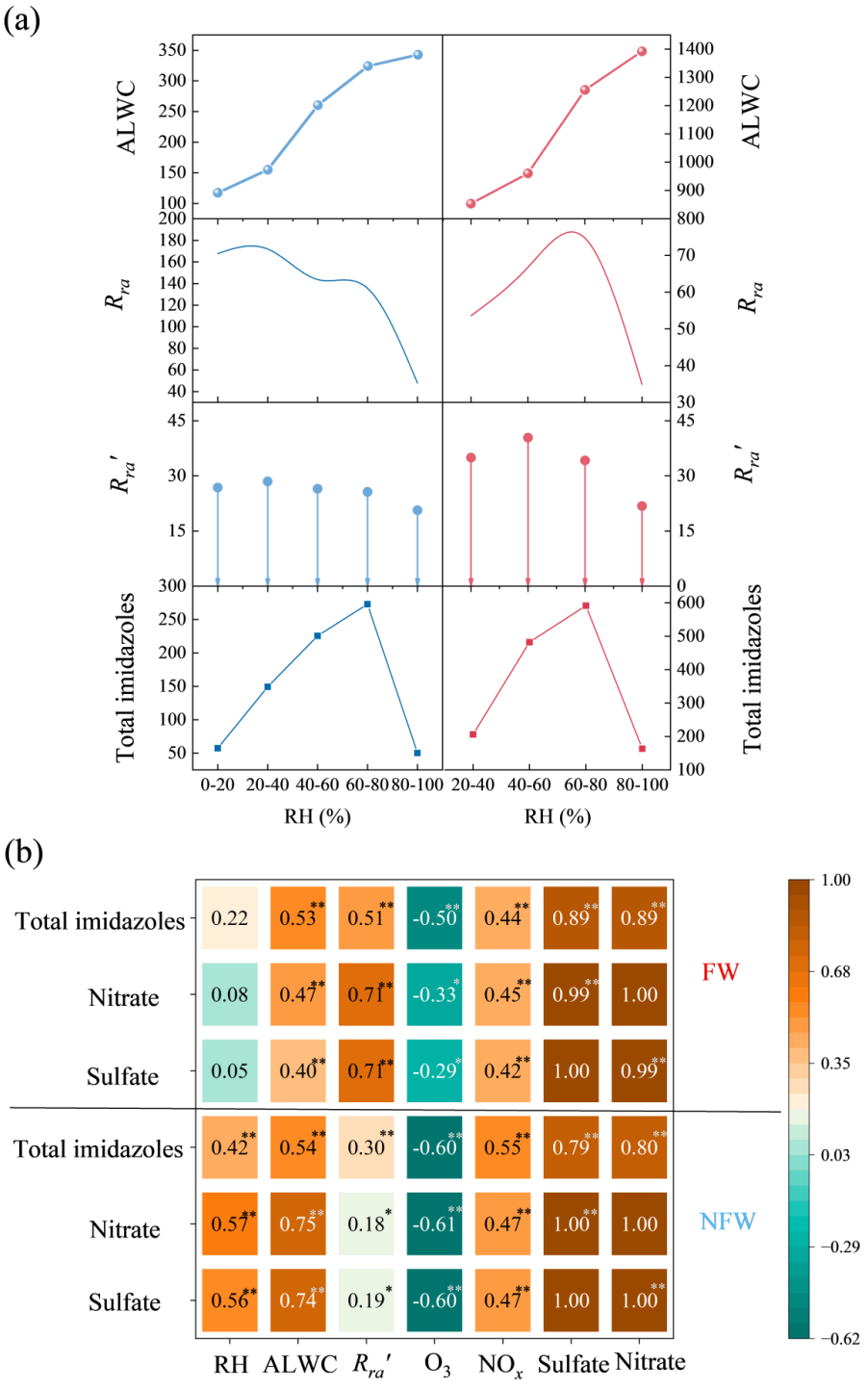


Figure 5. (a) Variations in aerosol liquid water content (ALWC), relative aerosol acidity (R_{ra}), modified relative aerosol acidity (R_{ra}'), and total imidazoles under varied relative humidity (RH) conditions during FW and NFW episodes; (b) correlation of nitrate, sulfate, and total imidazole-containing particles with R_{ra}', RH, ALWC and NO_x concentrations during the NFW and FW periods.

https://doi.org/10.5194/egusphere-2026-6959
Preprint. Discussion started: 20 November 2026
© Author(s) 2026. CC BY 4.0 License.

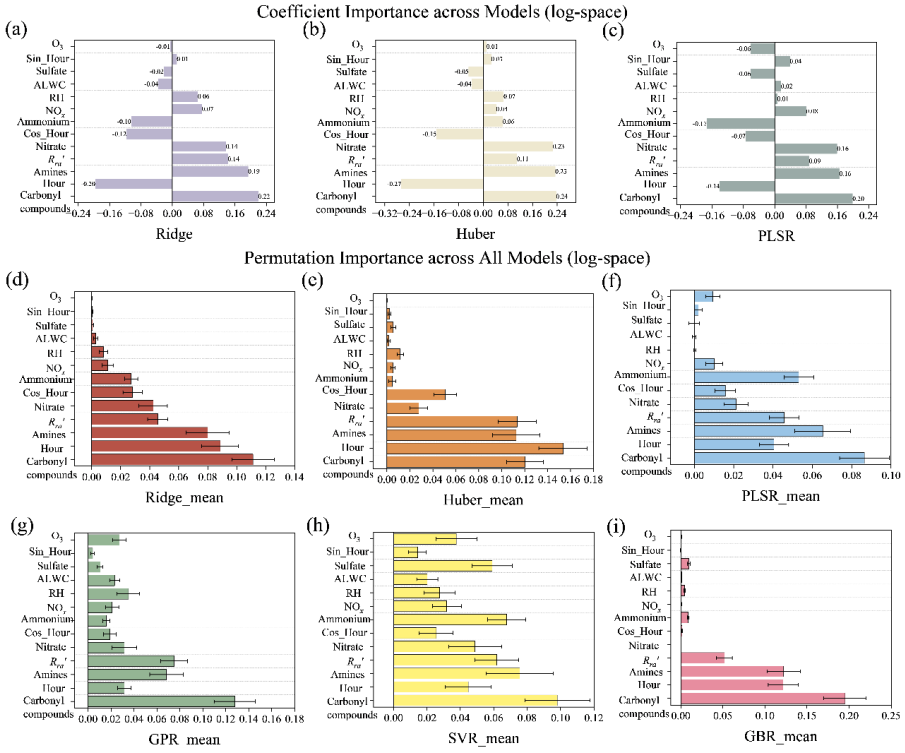


Figure 6. Comparison of feature importance for predictors of total imidazole-containing particles under logarithmic transformation. Standardized regression coefficients of 13 predictors in three linear models correspond to (a) Ridge, (b) Huber, and (c) PLSR, where bar length and direction represent the magnitude and sign of each variable's independent effect; (d–i) mean permutation importance of predictors from six base models correspond to (d) Ridge, (e) Huber, (f) PLSR, (g) GPR, (h) SVR, and (i) GBR. Error bars denote the standard deviation from repeated permutation sampling. All features are ranked by overall predictive contribution.